Sustainable Transportation Energy with Net Negative Greenhouse Gas Emissions: an Integrated Ecological and Engineering Systems Analysis

Final Report

17 December 2018

Investigators

University of Minnesota: Clarence Lehman, Professor, Ecology, Evolution, and Behavior, College of Biological Sciences; G. David Tilman, Regents Professor, Ecology, Evolution, and Behavior, College of Biological Sciences; Yi Yang, Post-Doctoral Researcher, Ecology, Evolution, and Behavior, College of Biological Sciences.

Princeton University: Anna K. Hailey, Graduate Researcher, Chemical and Biological Engineering; Thomas G. Kreutz, Senior Energy Systems Modeler, Andlinger Center for Energy and the Environment; Eric D. Larson, Senior Research Engineer, Andlinger Center for Energy and the Environment; Yueh-Lin Loo, Professor, Chemical and Biological Engineering; Johannes C. Meerman, Post-Doctoral Researcher, Andlinger Center for Energy and the Environment; Robert H. Williams, Senior Research Scientist, Andlinger Center for Energy and the Environment.

Colorado State University (subcontract): John Field, Research Scientist, Natural Resource Ecology Laboratory; Ernie Marx, Research Associate III, Natural Resource Ecology Laboratory; Keith Paustian, University Distinguished Professor, Department of Soil and Crop Science.

Abstract

This project assessed alternative bioenergy production and conversion systems with carbon capture and storage (BECCS) that might begin to be deployed commercially beginning in the relatively near term to help meet U.S. mid-century carbon-mitigation goals and transportation energy needs. The system-wide implications of two mechanisms for achieving negative greenhouse gas (GHG) emissions were assessed: geologic storage of CO_2 captured during feedstock conversion (CCS) and storage of photosynthetic carbon in roots/soil (R/S) during biomass production. The work was a collaboration between researchers at the University of Minnesota (UMN) and Princeton University (PU), with colleagues from Colorado State University (CSU) joining in the final year of the project.

Field experiments at UMN shed light on the ecological dynamics and R/S carbon storage potential of perennial grasses grown on agriculturally-degraded soils, of which there may be as many as 45 million hectares across the U.S. CSU researchers undertook high-resolution, national-scale modeling to estimate the potential for perennial grass production on such areas, including R/S carbon uptake. PU undertook techno-economic analysis of multiple bioenergy conversion technology pathways to understand comparative costs and benefits. PU integrated their findings with results from UMN and CSU to develop a national-scale assessment of the potential for BECCS systems to help meet mid-century U.S. transportation energy needs and carbon mitigation goals.

At UMN, the research quantified the aboveground biomass production and R/S carbon storage associated with production of switchgrass (in monoculture or in mixtures with legumes and/or C4 grasses) and with a high-diversity (32 species) mixture of native prairie grasses on degraded soils, each under alternative intensified cultivation practices, namely nitrogen fertilization and/or irrigation. Researchers seasonally collected data from experimental plots at the Cedar Creek Reserve, a site within the Long Term Ecological Research (LTER) Network. All intensification measures increased aboveground biomass production in the high-diversity experiment and all permutations of the switchgrass experiments, whereas for any given N or irrigation treatment, aboveground yields were about constant or lower with increasing species diversity. In switchgrass plots, adding legumes and/or C4 species had a slight negative impact on root biomass accumulation. Soil carbon storage rates in the upper 20 cm varied widely between plots with different species and between treatments. The highest rates were observed with the highest-diversity (32-species) plots under certain intensification practices. As a result, lifecycle greenhouse gas (GHG) emissions analysis of the production and conversion of biomass into electricity via co-firing with coal or into ethanol by enzymatic processing indicated that such high-diversity plots for the biomass production could yield GHG savings as high or higher than with the best-performing switchgrass monocultures.

At CSU, results from initial regional-scale ecosystem modeling work completed for this project suggest that large quantities of switchgrass can be produced on abandoned agricultural lands across the eastern US, but there are several dependencies and key uncertainties around achieving significant net greenhouse gas mitigation via photosynthetic R/S carbon storage. Down-scaling previous county-level estimates of abandoned land to the resolution required by the DayCent ecosystem model, it was estimated that 20.1–33.6 million hectares of abandoned land are available across the 37-state eastern US study area examined. If used to grow switchgrass with N fertilization

(75 kg ha^{-1}), these areas would produce 281–492 million metric tonnes per year of switchgrass. The simulations suggest that soil carbon would be sequestered at rates > 0.2 tC ha^{-1} y^{-1} across broad regions of the study area, but areas with coarse-textured soils or extreme climates in the Great Lakes, Southeast, and New England would have lower gains and in some cases losses. In addition, the high application rate of nitrogen fertilizer results in N_2O emissions that, across the 37-state region, offset the GHG benefit of carbon uptake by soils. The DayCent results are very sensitive to initial soil carbon levels, which are determined largely by what vegetation grew on the land during the 'idle' period after land abandonment and before bioenergy production started. Ongoing work is seeking to further refine the initial estimates.

PU researchers developed self-consistent techno-economic assessments of alternative processes for converting lignocellulosic biomass into liquid transportation fuels fungible with petroleum-derived fuels. The pathways included gasification- and hydropyrolysis-based systems, as well as microbial and catalytic conversion of sugars generated by enzymatic hydrolysis of biomass. For purposes of comparing alternative transportation energy systems, analyses were also developed for production from biomass of H_2 (for fuel-cell vehicles, FCVs) and of electricity (for EVs). Integrated CCS was investigated for each pathway, and a total of 14 process configurations were evaluated. Among options producing liquid fuels, hydropyrolysis configurations were found to give the highest liquid yields, while gasification and microbial processing provide the highest negative emissions per unit of biomass processed. Hydropyrolysis biofuels would be cost competitive with gasoline from $80/bbl crude oil in the absence of any GHG emissions price. Because of the high efficiency of FCVs and EVs, the bio-H_2 and bio-electricity options provide the lowest fuel cost per vehicle-km among all options investigated.

PU combined their technology pathway assessments with projections of sustainable biomass supplies in the US to estimate the contribution that biomass might make toward U.S. mid-century transportation energy needs and GHG emissions reductions goals. Crop residues (corn stover and wheat straw) and switchgrass from abandoned agricultural lands, as estimated in the work at CSU, were the biomass supplies considered. The analysis assumed that liquid biofuels would be used only for difficult-to-electrify transportation – air and heavy-road, rail, and water-borne freight – assuming all other transportation modes could be decarbonized via electrification. The PU analysis found that sufficient liquid biofuels could be produced with sufficiently low (or even negative) GHG emissions that a 2050 U.S. GHG emissions target consistent with the goals of the Paris Climate Accord could be met.

PU researchers also made a preliminary assessment of the pace at which such an advanced liquid biofuel industry might plausibly develop. The scale of that industry at its largest would be about 4 times that of today's U.S. corn-ethanol industry on the basis of liquid fuel output, but due to the lower volumetric energy density of baled crop residues and switchgrass compared with corn grain, the volume of biomass handled would be 27 times that of today's corn-ethanol industry. Government incentives much stronger than those that drove expansion of the U.S. corn-ethanol industry would likely be needed to drive commercial deployment of an advanced biofuels industry at the pace and scale needed to achieve U.S. 2050 GHG emissions targets.

Introduction

In its 5th Assessment Report [1] the International Panel on Climate Change (IPCC) articulated the imperative of deploying negative greenhouse gas (GHG) emissions technologies for there to be a reasonable probability of limiting global warming to 2°C or less above the pre-industrial level, the goal stipulated in the Paris Climate Accord. The IPCC identified systems that use non-food biomass for energy with CO_2 capture and storage (BECCS) as important for achieving negative emissions. The recent IPCC special report on the impacts of global warming of 1.5°C [2] draws further attention to the role that BECCS plays in some scenarios.

This is the final report on a collaboration between researchers from the University of Minnesota and Princeton University to assess alternative BECCS systems that might be deployed commercially in this half century to help meet U.S. mid-century carbon-mitigation goals and transportation energy needs. A key aspect of the work was understanding system-wide implications of two mechanisms for achieving negative greenhouse gas (GHG) emissions: geologic storage of CO_2 captured during feedstock conversion (CCS) and storage of photosynthetic carbon in roots/soil (R/S) during biomass production. The fundamental science that was advanced is a new understanding of the ecological dynamics and R/S carbon storage potential of perennial grasses grown on the significant hectares across the U.S. characterized by degraded soils ill-suited for conventional agriculture. This understanding was integrated with analysis of energy conversion technology pathways to understand costs and benefits of alternative BECCS systems for meeting mid-century U.S. transportation energy needs and carbon mitigation goals.

Previous annual progress reports [3,4] and prior publications (see list below) describe work carried out over the first two years of the project. This report summarizes work over the final 16 months. During this period, researchers from Colorado State University joined the collaboration under subcontract to the University of Minnesota.

Results

1 The University of Minnesota

The research at Minnesota examined the effects on perennial bioenergy grass production on degraded soils of intensified cultivation, including nitrogen fertilization and irrigation and of species diversity, particularly with respect to aboveground biomass production and root/soil carbon storage. The third year of the project at Minnesota saw further sampling of aboveground biomass, total root biomass, and soil carbon concentration in two experiments involving intensification at the Cedar Creek Ecosystem Science Reserve, a site within the Long Term Ecological Research (LTER) Network. The collected data were analysed, and life-cycle GHG emission savings were quantified using two common bioenergy conversion scenarios: co-firing with coal to generate electricity and converting to cellulosic ethanol. The team at Minnesota also worked closely with the team at Colorado State University, supplying experimental data for calibrating their DayCent modelling aimed at estimating the potential for bioenergy grasses grown on degraded lands nationwide.

1.1 Experimental sampling

During the 2017 field season, sampling was conducted for two experiments at Minnesota:

- High-diversity prairie experiment: to test effects of irrigation and fertilization on productivity and soil carbon storage in plots planted with 32 native grassland species
- Switchgrass experiment: to test effects of irrigation, fertilization, and plant diversity on productivity and soil carbon storage in plots planted with switchgrass monoculture and mixtures.

We sampled each plot in early to mid-August, the time of peak living biomass at our site, for aboveground biomass production. In each plot, we clipped four parallel and evenly spaced 10 cm wide by 600 cm long strips of vegetation, dried the vegetation at 40° C, and weighed to determine the amount of biomass produced. We also sorted biomass from one of the four clipped strips by species before drying to determine plant diversity. Next, we sampled each plot for total root biomass. We collected cylinders of soil samples 5 cm in diameter and spanning from 0-30 cm depth and 30-60 cm depth, at eight locations evenly spaced within the strips that we had clipped. We rinsed each soil core with a gentle water spray on a fine mesh screen to remove soil, dried the roots at 40° C, placed them in a sieve and shook gently to remove any remaining soil, and then weighted to determine total root biomass. Last, we sampled each plot for soil carbon concentration. We took nine soil cores in each plot, each soil core being 2.5 cm in diameter and spanning the upper 0-20 cm soil depths. We first sieved each soil core to remove roots and then combined and thoroughly mixed all nine cores from a plot. Next, we dried and mixed the soil samples again, and subsamples were ground for C measurements and other subsamples were archived. Finally, we dried the ground samples again at 104° C and then analysed for total C by combustion and gas chromatography (Costech Analytical ECS 4010 instrument, Costech Analytical Technologies Inc., Valencia, CA).

1.2 Experimental results

Key results from the two switchgrass and high-diversity experiments are shown in Figure 1.

Nitrogen addition and irrigation each increased aboveground biomass production, whereas for any given treatment, yields were about constant or lower with increasing species diversity (Figure 1A). In the switchgrass experiment, using data for years 2015 to 2017, plots with 7 g m^{-2} of N addition produced 532 (±23) g m^{-2} of aboveground biomass per year as opposed to 423 (±15) g m^{-2} for those without N. And plots with irrigation produced 541 (±22) g m^{-2} of aboveground biomass, as opposed to 413 (±15) g m^{-2} for those without irrigation. Similarly, in the high-diversity experiment, plots with 7 g m^{-2} of N addition produced 466 (±43) g m^{-2} of aboveground biomass per year as opposed to 371 (±34) g m^{-2} for those without N, and plots with irrigation produced 519 (±31) g m^{-2}, as opposed to 317 (±26) g m^{-2} for those without irrigation. Provided the positive effect of intensification, treatments that produced the highest yields were those receiving both N and irrigation, specifically 648 (±67) g m^{-2} for switchgrass plus legume (SG+L), 645 (±68) g m^{-2} for switchgrass plus two other C4 grasses (SG+C4), 615 (±63) g m^{-2} for

switchgrass monocultures (SG), 587 (±32) g m^{-2} for the 32-species, and 556 (±56) g m^{-2} for switchgrass plus legume and the C4 grasses (SG+C4+L).

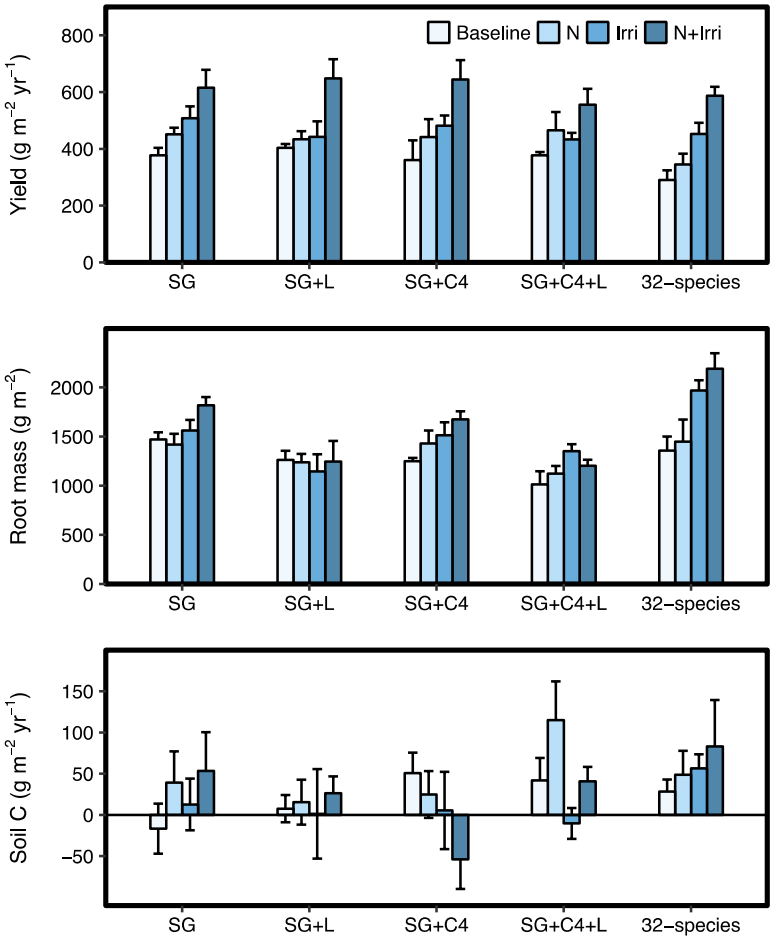

Figure 1. Key results from switchgrass and high-diversity experiments: average aboveground biomass (or yield) of the past three years from 2015 to 2017 **(A)**, total root biomass in upper 60 cm of soil measured in 2017 **(B)**, and soil carbon storage rates in upper 20 cm of soil **(C)**. SG: switchgrass monocultures; SG+L: switchgrass plus legume; SG+C4: switchgrass plus two other C4 grasses; SG+C4+L: switchgrass plus legume and the C4 grasses. The 32-species treatment is from the high-diversity experiment[a]. Baseline: no N addition nor irrigation; N: 7 g m^{-2} of N addition only; Irri: irrigation only; N+Irri: both N addition and irrigation. Bars are means with standard errors.

In the switchgrass experiment, root biomass accumulated in smaller amounts in plots with legumes present (Figure 1B). Switchgrass plus legumes (SG+L) and the most diverse treatment (SG+C4+L) accumulated 1223 (±68) g m^{-2} and 1173 (±51) g m^{-2} of total root biomass, which were significantly (P=0.5) lower than that of switchgrass monocultures (SG; 1567 (±58) g m^{-2}) and switchgrass with C4 mixtures (SG+C4; 1467

[a] Yang Y Tilman D Lehman C Trost JJ 2018 "Sustainable intensification of high-diversity biomass production for optimal biofuel benefits" Nature Sustainability [in press]

(±61) g m^{-2}). The 32-species high-diversity plots were planted earlier than the switchgrass plots (2007 vs 2012), and thus have generally accumulated more root biomass (1742 (±105) g m^{-2}). A long-term biodiversity experiment at University of Minnesota shows roots can grow for 2 decades [5], albeit at decelerating rates, so more root biomass is expected for both switchgrass and high-diversity experiments.

Soil carbon (C) sequestration rates (0-20 cm) varied widely between plots within a treatment and between treatments (Figure 1C). In the switchgrass experiment, several treatments lost soil C compared with the baseline carbon stocks measured before the experiment, and some stored only small amounts (1 to 8 g-C m^{-2} yr^{-1}). Nine out of the sixteen diversity-intensification treatments stored moderate amounts of soil C, from 13 to 53 g-C m^{-2} yr^{-1}, and the switchgrass plus legume and C4 with N addition stored the most (115 g-C m^{-2} yr^{-1}). The four treatments in the high-diversity experiment stored 28, 29, 57, and 83 g-C m^{-2} yr^{-1} of soil C, respectively (Figure 1C). Across diversity treatments, the higher diversity treatments, SG+C4+L and 32-species, stored in general more soil C than the rest (42 and 54 vs 22, 13, and 7 g-C m^{-2} yr^{-1}).

1.3 Life-cycle GHG savings

Converting the aboveground biomass in our experiments to bioenergy to displace fossil fuels would result in net GHG savings for most treatments (Figure 2), and GHG savings from high-diversity treatments could be as great or greater than those from switchgrass monocultures, depending on the intensification level. The amount of GHG savings depends on the fossil fuel displaced and varies between treatments given differences in soil/root carbon storage and aboveground biomass yield. In the two bioenergy scenarios we examined, the best performing treatments are those that had high yields and/or large root/soil C storages (Figure 2A). Treatments that lost a large amount of soil carbon could result in negative GHG savings, as in SG+C4 case with N and irrigation when converted to ethanol. In this case, GHG savings from ethanol displacement would be more than negated by carbon losses from the soil. In the scenario of co-firing biomass with coal to generate electricity, some of the higher diversity treatments (SG+C4+L with N and 32-species with N and irrigation) would result in as much GHG savings as would the best-performing switchgrass monocultures (1082 and 1165 vs 1085 g CO_2e m^{-2} yr^{-1}). In the ethanol scenario, these high diversity treatments would result in much greater GHG savings than the best-performing C4 monocultures (501 and 432 vs 316 CO_2e m^{-2} yr^{-1}). These results highlight the benefit of high plant diversity for climate change mitigation potentials of bioenergy from perennial grasses.

1.4 Publications, manuscripts

The research at Minnesota is reported in published [6], submitted [5], and in-preparation [7,8] manuscripts.

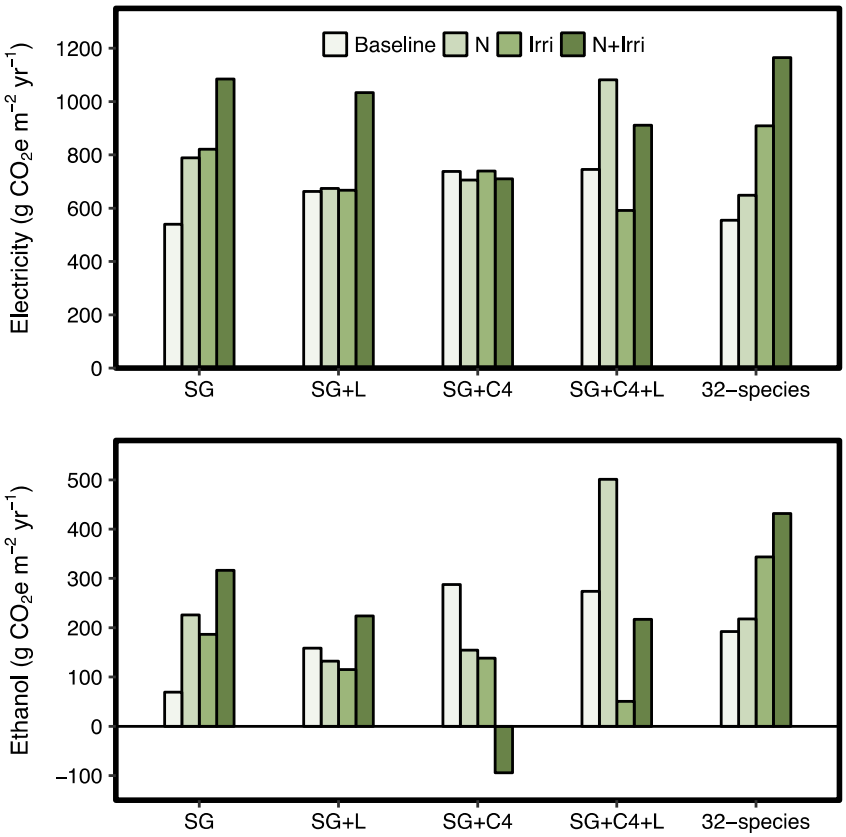

Figure 2. Potential life cycle GHG savings from two bioenergy scenarios: co-firing with coal to generate electricity (**A**) and cellulosic ethanol (**B**). The estimates include 1) foregone C, that is, C that would have been stored in soil and roots without land conversion or if the abandoned land had continued to undergo natural succession and 2) avoided GHG emissions from coal (in **A**) and gasoline (in **B**), assumed to be displaced by the bioenergy produced on an energy-equivalent basis.

2 Colorado State University

Researchers at Colorado State University (CSU), led by Dr. John Field, joined the Minnesota-Princeton collaboration as subcontractors to Minnesota for the final year of the project. The main objective of the added contributions from CSU was to scale up results from the Minnesota field experiments (and other relevant field experiments) to estimate the potential across the U.S. for biomass production and soil carbon sequestration on abandoned agricultural lands, estimates that Princeton researchers used in analysis (described in Section 3) to estimate contributions that biofuels might make toward meeting mid-century U.S. transportation energy needs and carbon mitigation goals. The CSU researchers have summarized their work in the following sections.

2.1 Introduction

We used spatially-explicit ecosystem process modeling to predict the productivity and soil greenhouse gas (GHG) emissions balance of cultivating switchgrass on abandoned agricultural land across the Eastern United States. Our Eastern US study area was defined to include the Dakotas, Nebraska, Kansas, Oklahoma, Texas, and all states to the east (37

states and 2,481 counties in total). Soil GHG balance is determined by carbon dioxide (CO_2) exchange associated with net changes in soil organic matter (specifically soil organic carbon, or SOC) levels over time, as well as fluxes of trace gases such as nitrous oxide (N_2O) and methane (CH_4). The net soil GHG balance of cultivating dedicated biomass feedstock crops varies widely as a function of climate, soils, land use history, and management intensity, with important implications for the GHG intensity of resulting bioenergy products [9]. Using a spatially-explicit ecosystem process model allows us to predict how switchgrass productivity and associated soil GHG balance is likely to vary at landscape and regional scale due to climatic gradients and spatial heterogeneity in soil properties and land use history, and in response to different management practices.

2.2 Methods

2.2.1 DayCent and workflow overview

We used the DayCent biogeochemistry model to simulate switchgrass productivity and associated soil GHG balance. DayCent is a deterministic, process-based model that represents the dynamics of carbon (including net primary production, photosynthate allocation to different plant tissues, plant phenology and tissue death, and stabilization of organic matter as SOC) and coupled nitrogen and water cycling in both natural and agricultural ecosystems (Figure 3). These processes are simulated as a function of plant cover type, management practices, and site-level climatic and soil edaphic factors. DayCent is based on the older CENTURY model, which was originally designed to predict spatial trends in grassland soil carbon in the US Great Plains region [10]. CENTURY represents soil carbon dynamics using three conceptually-defined SOC pools with different inherent residence times (active, slow, passive), a convention now widely adopted among other SOC models [11]. DayCent updates CENTURY with a daily time-step and more detailed representation of hydrological and nitrogen cycles in order to better represent trace GHG emissions [12].

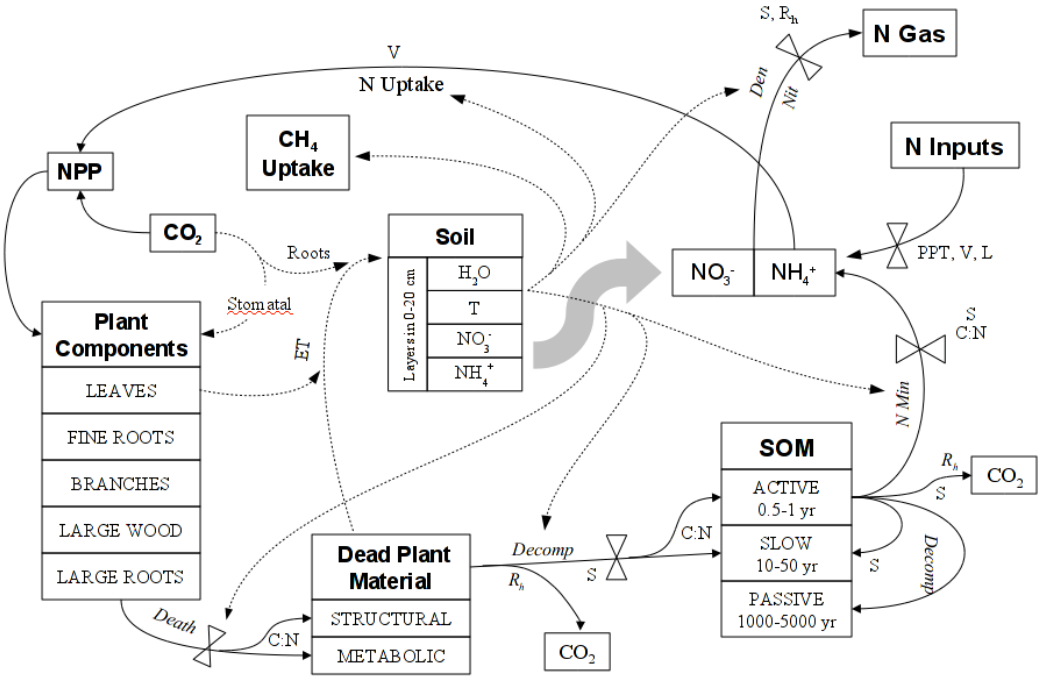

Figure 3. DayCent model conceptual schematic illustrating key processes represented.

DayCent requires input data on soil texture as a function of depth, which acts as a primary control of water and nitrogen dynamics and the microbial efficiency of SOC stabilization. The other primary input data requirements are site latitude, daily weather (minimum and maximum air temperatures and precipitation totals), and approximate land use history. The model requires initialization in order to establish the pre-settlement equilibrium values for the three different conceptual SOC pools, and to represent historic changes in SOC levels in response to human management (plow-out and row crop cultivation, animal grazing, etc.). Our analysis workflow involved the following basic steps:

1. Identification of abandoned land areas
2. Estimating land use history of those areas
3. Executing and analyzing regional-scale simulations

2.2.2 Identification of the abandoned land base

Estimates of marginal, abandoned, degraded land availability vary widely [13], due in part to different and often divergent functional definitions. For this analysis we have chosen to focus on abandoned agricultural lands in the US as assessed by [14]. Those authors reviewed agricultural land use statistics to determine if and when the total extent of cropland and pastureland peaked in each county in the US, and how much it has declined since that peak. They estimated that total agricultural land area in the US peaked in the 1940s, and then declined by 68 million hectares (Mha) as of the year 2000. They down-scaled these county-level estimates to a gridded map of 5-minute spatial resolution (~8-mile grid size) using a back-stepping algorithm initialized with current-day agricultural land distribution. After excluding areas within each grid cell that may have become developed or re-forested, the authors estimate that 45 Mha of abandoned agricultural land remains in a state that could be appropriate for bioenergy uses.

DayCent requires even finer down-scaling in order to specify individual soil profiles and other input data needed to drive simulations. We have previously developed a high-resolution GIS intersect of standard US soil, climate, and land cover data in order to specify DayCent model runs for individual sub-field-scale land parcels across the continental US, as described in [15]. In order to represent the estimates of [14] of abandoned land within this system, we first re-aggregated their 5-minute data (downloaded from http://portal.nersc.gov/project/m2319/AbandonedAG/download.html) back to the native county level. Next, we used the 2011 National Land Cover Database (NLCD; [16]) to identify the land parcels in each county with modern-day land cover that could be consistent with the definition of [14] of bioenergy-available abandoned agricultural land. Specifically, we assumed that land classified in the 2011 NLCD as shrubland or herbacious natural vegetation could be consistent with a previous history of agricultural use and abandonment, but that other land covers were likely never cultivated (water, wetlands, barren classifications) or cannot be considered bioenergy-available (forested and developed classifications). The NLCD category of pasture/hay land cover is defined broadly enough that it is ambiguous whether such areas should be considered cropland, or could be consistent with a previous history of agricultural use and abandonment; we therefore performed different versions of the analysis with this pasture/hay land either included or excluded in order to provide upper and lower bounds for abandoned land availability.

We created an algorithm to iterate through each county in our Eastern US study area and randomly designate such 'eligible' land parcels from our GIS intersect as 'bioenergy-available abandoned agricultural land', until either the county target abandoned land area was satisfied or the county ran out of eligible land. The results of this down-scaling are shown in Figure 4. The more conservative assumption that current-day pasture/hay is ineligible to be considered 'abandoned' results in many counties in the upper mid-west and Mississippi River valley running out of eligible land before the total target area is achieved (a). Relaxing that constraint resulted in the target level of abandoned land being designated in most counties, except for those in the lower Mississippi River valley (b). The resulting county-level abandoned land availability is shown in panels (c) and (d). When pasture/hay land is excluded from consideration, our algorithm identified a total of 20.1 Mha of down-scaled bioenergy-available abandoned land in our Eastern US study area, much of it concentrated in the central Great Plains region (c). In contrast, when pasture/hay is included, additional abandoned land can be designated in significant concentrations in New York, Pennsylvania, and the interior Southeast, for a total of 33.6 Mha.

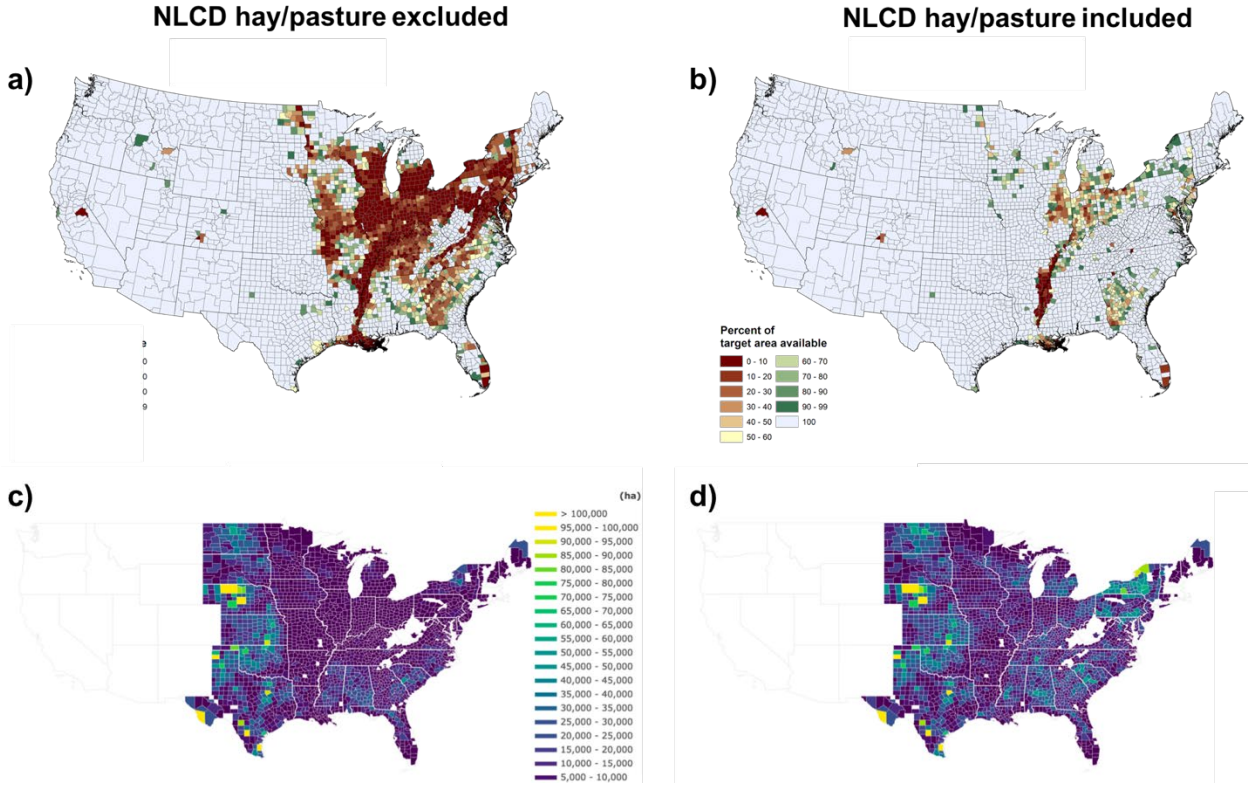

Figure 4. Maps showing county-level bioenergy-available abandoned agricultural land area estimates from Zumkehr & Campbell 2013, after custom down-scaling based on NLCD land cover.

2.2.3 Estimating land use history

Our typical DayCent model workflow leverages an archive of model initialization states based on the same standard assumptions around pre-settlement vegetation distribution and historic land use trends used in the annual Inventory of U.S. Greenhouse

Gas Emissions and Sinks [17]. The present analysis relied on that resource to estimate historic SOC depletion from agriculture, and the equilibrium value of SOC at the time of land abandonment. That simulation starting point was then appended with a simulation of the land 'idle' period after abandonment and before switchgrass cultivation. Previous sensitivity analysis (not shown) showed that the degree of SOC recovery during the idle period is highly dependent on the length of and assumed land cover during that period. This in turn determines the starting SOC level at the time of switchgrass establishment, which strongly influences the degree to which SOC will accumulate or decline during switchgrass cultivation.

The typical length of land idle period was extracted from the data of [14] for each county. We assumed that land area decreased linearly from the year of peak extent to the year 2000, and thus a representative land idle period was exactly half of that time. We did not attempt to model idle periods of longer than 50 years, assuming that SOC would come to equilibrium by that time. We assumed a land cover of native grassland during that period, with annual low-intensity livestock grazing. While other studies have suggested that there is likely significant delay in native plants re-colonizing the bare abandoned land, we have not yet identified sufficient data with which to parameterize such a delay. Instead, we made the conservative assumption of no re-colonization delay, i.e., that seed dispersion will be ample to support development of a full plant canopy immediately after land abandonment.

It is increasingly common for bioenergy lifecycle assessment studies to evaluate the GHG impacts of feedstock production in relative terms against a business-as-usual land use baseline. However, our initial exploratory analysis suggested that this type of relative GHG accounting exacerbated the sensitivity of our analysis to the poorly-constrained assumptions of idle-period land cover described in the previous paragraph. We are continuing to seek a better data-grounded basis for making an assessment on a relative basis. In the meantime, the GHG balance results presented here are on an absolute basis.

2.2.4 Executing regional-scale simulations

Our analysis used previously-developed DayCent switchgrass calibrations as described in [15]. That effort produced national-scale calibrations for both upland and lowland switchgrass ecotypes using secondary field trial data from the literature, including field trials on marginal land where available. The resulting upland and lowland calibrations were evaluated using holdout validation, which demonstrated r-values of 0.26 and 0.66, and root mean squared error values of 3.7 and 4.1 Mg ha^{-1}, respectively. Work to mobilize the field trial data from the Cedar Creek LTER site described previously for further DayCent model validation – and the calibration of a mixed prairie land cover to contrast with commercial switchgrass monocultures – is ongoing.

The current analysis assumes the cultivation of upland switchgrass varieties at latitudes above 40 °N, and lowland varieties below. We assumed non-irrigated switchgrass cultivation, with annual application of nitrogen fertilizer at a rate of 75 kg N ha^{-1}. This value is at the high end of the range encountered in the switchgrass field trials compiled in [15], the data for which is available at https://doi.org/10.6084/m9.figshare.5436313.v1. This analysis also assumed that switchgrass fields are replanted every 10 years, with medium-intensity tillage operations

during field preparation, and no fertilizer application or biomass harvest in the establishment year.

The down-scaling exercise described above identified 344,292 different DayCent simulations required to represent the spatial heterogeneity of abandoned agricultural lands across our 36-state study area. These model runs were executed in parallel across a high-performance computing cluster at the Colorado State University Natural Resource Ecology Laboratory using previously-developed Python (http://www.python.org/) code for input data management, model execution, and aggregation of results. That code had to be updated in two ways to support the current analysis:

1. In order to represent regional variation in switchgrass phenology, beginning-of-season green-up dates and end-of-season senescence dates were set individually for each simulation as a function of site latitude, as per Figure 5.
2. The length of the 'idle period' after land abandonment and before switchgrass cultivation was set individually for each simulation as described in the previous section.

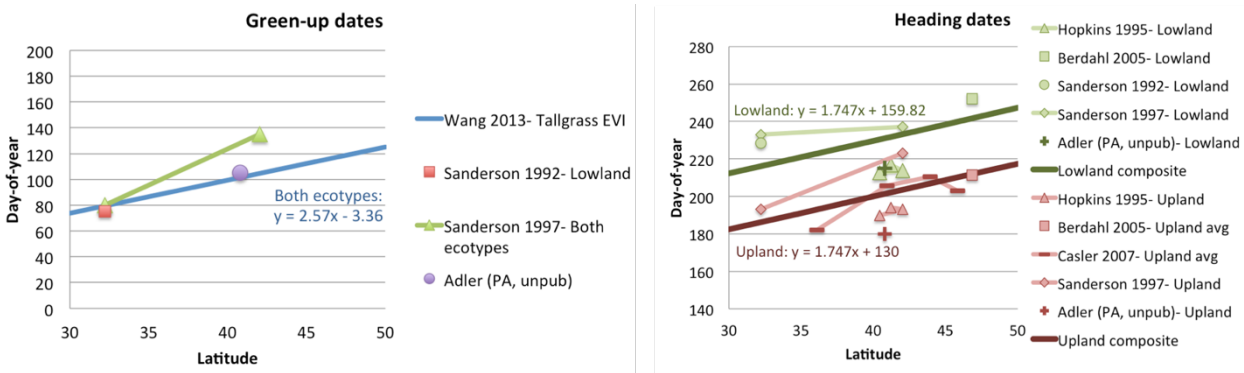

Figure 5. Green-up and heading (i.e., flower/seed-head emergence) dates for upland and lowland switchgrass varieties as a function of latitude, reproduced from the Online Supplemental Information section of [15]. Senescence was modeled to occur three weeks after the heading date.

Custom code was written in the Pandas module (https://pandas.pydata.org/) to perform the following operations on the raw DayCent model output:

- Aggregating results to single time-averaged values for each scenario.
- Converting DayCent results in native (g m^{-2}) units to more standard (Mg ha^{-1}) units.
- Estimating indirect N_2O fluxes from ammonia volatilization, nitrate leaching, and nitric oxide emissions results.
- Assigning CO_2-equivalent values to all fluxes of N_2O (265) and CH_4 (28) as per the 100-year global warming potentials (GWP) reported in the Fifth Assessment Report of the Intergovernmental Panel on Climate Change [18], and combining to determine the net soil GHG balance of each simulation.

Finally, choropleth maps of select yield and GHG results were produced via the Plotly visualization library (https://plot.ly/python/).

2.3 Results

Table I presents a summary of DayCent simulation results across the Eastern US study region for the bounding cases where NLCD pasture/hay areas are and are not considered eligible for designation as abandoned land (see 'Identification of the abandoned land base' section and Figure 4 above). While per-area switchgrass yield and soil carbon performance are relatively constant across the two scenarios, including pasture/hay areas increases the total amount of land we can simulate as abandoned by a factor of 2/3, and thus increases total study area biomass production and carbon sequestration by similar amounts. In both scenarios, direct and indirect emissions of nitrous oxide from microbial nitrification and denitrification processes are large enough on average to more than cancel out the soil carbon sequestration and methane oxidation effects, leading to a net positive soil GHG balance.

Table I. Summary of DayCent-simulated switchgrass performance for the entire Eastern US study area.

	NLCD pasture/hay excluded	**NLCD pasture/hay included**
Land availability (Mha)	20.1	33.6
Average switchgrass area yield (Mg ha^{-1} y^{-1})	14.0	14.6
Total biomass production (Mt y^{-1})	281	492
Average SOC area increase (Mg C ha^{-1} y^{-1})	0.07	0.06
Total soil carbon increase (Mt C y^{-1})	1.39	2.03
Total net soil GHG emissions (Mt CO_2e y^{-1})*	2.76	7.40

*Positive values mean soil N_2O emissions (direct + indirect) out-weigh carbon uptake + methane oxidation.

2.3.1 Regional patterns in yield and GHGs

The average numbers presented in the previous section gloss over important regional variations in switchgrass performance. Figure 6 shows simulated switchgrass yields alongside the temperature and precipitation gradients across our study area. Note the discontinuity in yields at 40 °N (the boundary between Kansas and Nebraska) associated with the threshold between upland and lowland variety cultivation ranges. These results suggest that temperature and precipitation are adequate to support lowland variety yields in excess of 18 Mg ha^{-1} y^{-1} across a wide area from eastern Kansas to southern Indiana to Louisiana. Yields decline precipitously west of the 100th meridian due to precipitation limitations. These results compare well to other recent switchgrass yield predictions based on a synthesis of field trial results and environmental limitation mapping using a combination of process-based modeling and expert judgement [19,20].

DayCent predictions of soil GHG fluxes are strongly affect by soil texture in addition to climate (Figure 7, panel **a**). Our study area includes distinct pockets of coarse sandy soils in Michigan and the Great Lakes region, in Florida, and in the Sand Hills region of Nebraska. While many areas show soil carbon sequestration at rates of 0.1 Mg C ha^{-1} y^{-1} or greater (**b**), these sandy areas require significant inputs of litter carbon to maintain SOC levels despite low microbial stabilization efficiencies, and thus show soil carbon declines under switchgrass cultivation for bioenergy (where all aboveground biomass is assumed to be removed for harvest). Direct nitrous oxide emissions are the other large

determinant of the net soil GHG balance, and tend to be highest on the moderately-texture soils of the Mid-West, New England, and the Mississippi River valley (**c**). The CO_2-equivalent GHG emissions of N_2O often exceeds that of carbon sequestered in the soil, and thus only limited areas in the lower Mid-West and Great Plains experience a net negative soil GHG balance (**d**).

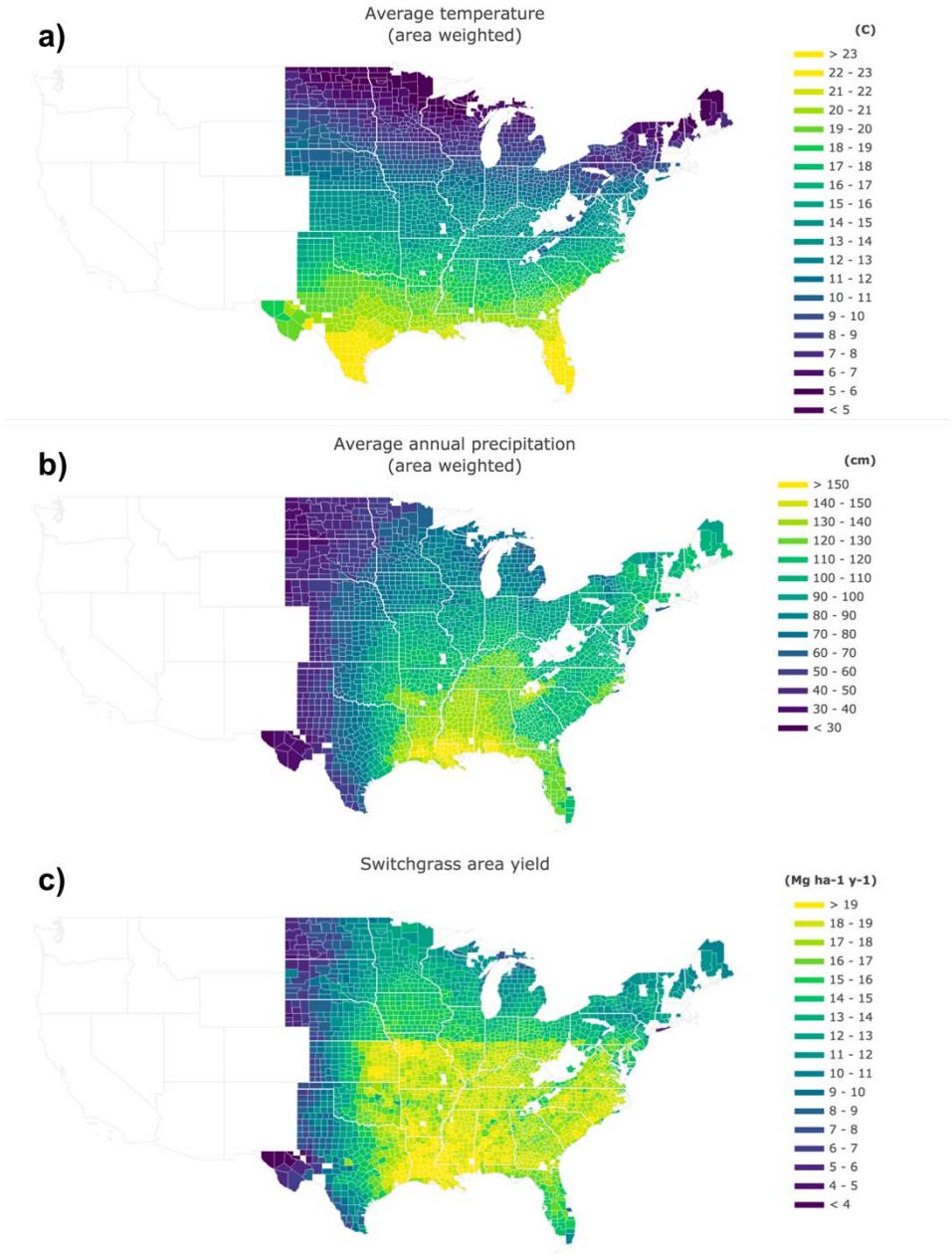

Figure 6. Regional gradient in temperature (a) and precipitation (b), and DayCent-predicted average annual switchgrass yields (c).

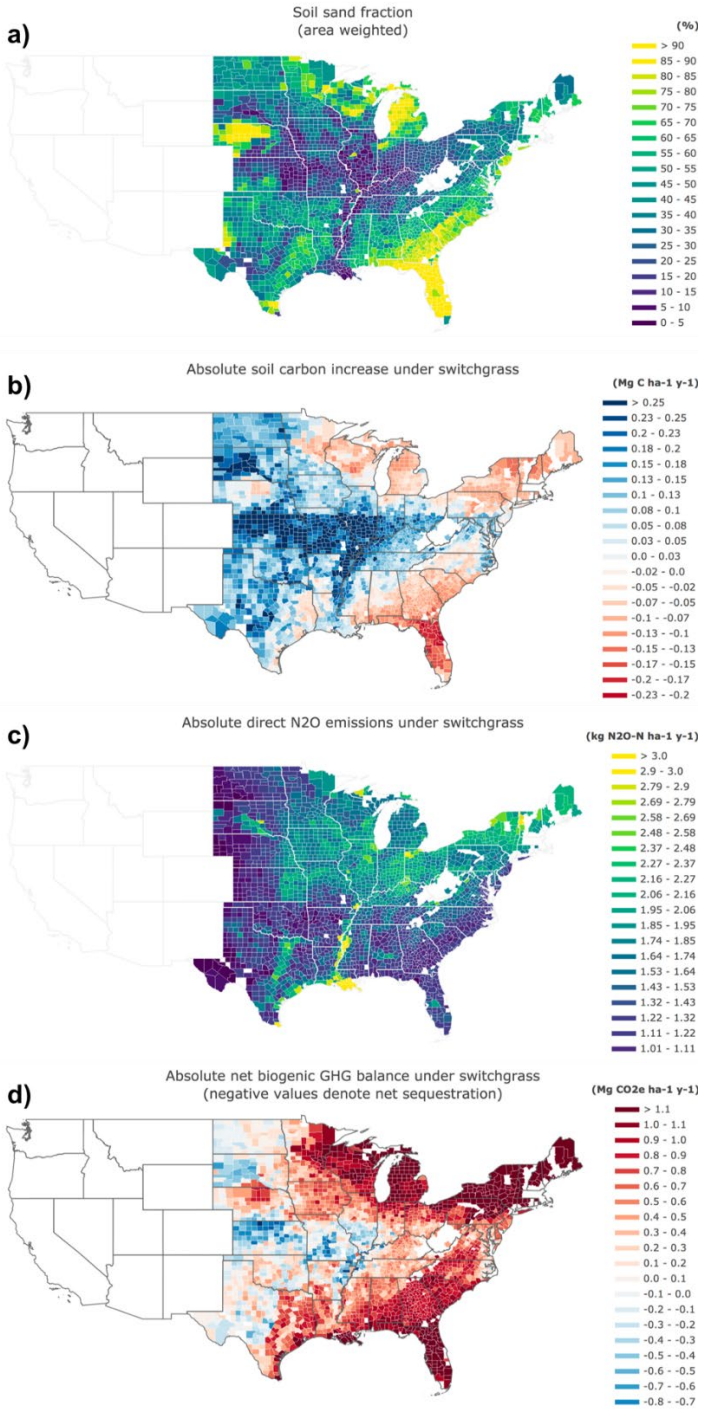

Figure 7. Regional heterogeneity in soil surface texture (a), and DayCent-predicted absolute soil carbon change (b), direct nitrous oxide emissions (c), and net soil GHG balance (d) under switchgrass cultivation.

Of course, these per-area yields and GHG balances are only realized in the areas of abandoned agricultural land where switchgrass might be cultivated. Figure 8 shows the intersection of the abandoned land availability under different scenarios illustrated in Figure 4 with the per-area soil carbon outcomes mapped in Figure 7. Under more

conservative assumptions (Figure 8a), the concentration of abandoned land in the Great Plains region aligns reasonably well with areas of high soil carbon sequestration potential (though the western areas in that range are marginal on yield). In contrast, more liberal assumptions around abandoned land availability (Figure 8b) introduce new areas in the Nebraska Sand Hills, New York, and the Southeast are introduced and that are likely to have poorer soil carbon sequestration outcomes.

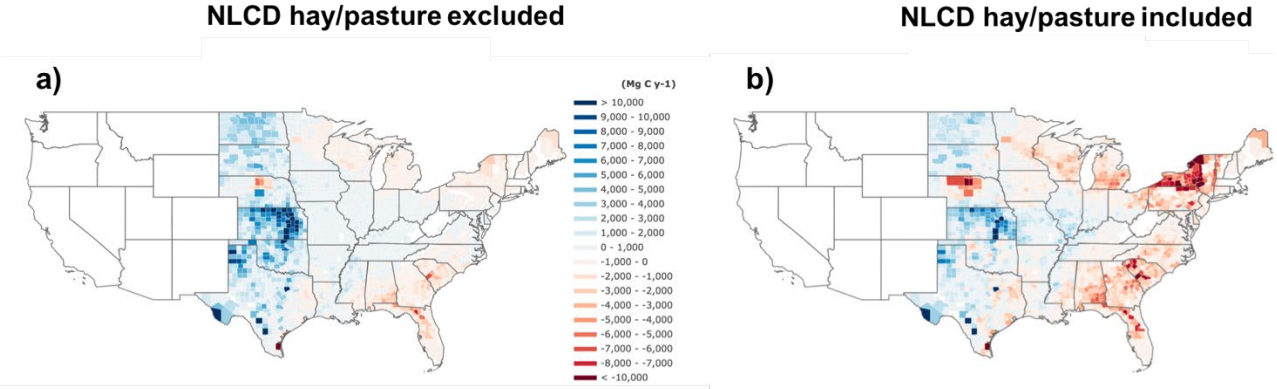

Figure 8. Absolute soil carbon changes realized under switchgrass cultivation, assuming that current-day hay/pasture land is ineligible (a) or eligible (b) for designation as abandoned.

2.4 Conclusions and ongoing work

We acknowledge that significant discrepancies remain around identifying the abandoned agricultural land base at a functional level, and in representing idle-period land cover dynamics in sufficient detail to produce reliable estimates of soil carbon trends prior to switchgrass cultivation. However, the results generated so far highlight inter- and intra-regional variability in the net GHG balance of switchgrass cultivation. This variability provides a basis and opportunity for policy design to support regionally-appropriate land uses and landscape optimization [9], focusing production practices on the areas most likely to achieve positive environmental outcomes.

Our ongoing work is focusing on better characterizing and modeling the dynamics of re-colonization of bare abandoned land by native plants, leveraging secondary literature we can identify on the topic. We will also experiment with simulating N application rates that are tailored to the yield potential at a given site, rather than a conservatively-high uniform rate. In addition, other collaborations are providing phenotypic performance data for new switchgrass varieties, which – if they can be adequately represented via model recalibration – can provide the basis of studying phenotype – environment interactions, and bioenergy landscape design based on matching the most appropriate variety with the most appropriate management for a given planting location.

3 Princeton University

Work at Princeton in the full course of the project included process design and techno-economic analysis of multiple advanced biomass conversion technology pathways and self-consistent comparisons among these. Results from the techno-economic assessments were combined with preliminary mid-century projections of the availability

of domestically-produced sustainable biomass supplies in the US to gain some insight into the contribution that biofuels might make toward U.S. transportation sector energy needs and GHG emissions reductions. The biomass feedstock supply in this analysis focused on feedstocks that would minimize indirect land-use change GHG emissions: crop residues (corn stover, wheat straw) and perennial grasses cultivated on abandoned agricultural lands (as estimated by the work at CSU). Princeton researchers also evaluated the pace at which a U.S. lignocellulosic biofuel industry might plausibly develop, with comparisons to the pace envisioned for U.S. transportation system emissions mitigation in many integrated assessment model scenarios that limit global average temperature rise to no more than 2°C.

3.1 Biofuel production systems design and performance estimates

Much of Princeton's effort during the project focused on comparative assessments of the prospective technical, economic, and environmental performance of multiple technological pathways for converting lignocellulosic biomass into liquid transportation fuels fungible with petroleum-derived fuels. The potential for incorporating capture and geologic storage of byproduct CO_2 was also investigated for each pathway. Alternative process designs were simulated using Aspen Plus software. In combination with Princeton's extensive in-house capital and operating cost database for energy conversion processes, this represents a harmonized methodology for self-consistent technical, economic and environmental performance comparisons among different pathways.

Earlier work in the project evaluated gasification and pyrolysis-based systems, including potential synergies of co-feeding with coal or natural gas. This work was described in prior annual progress reports [3,4] and publications [21,22,23]. In the final year, assessments were undertaken of additional pathways involving biological or catalytic conversion of sugars generated via pretreatment and enzymatic hydrolysis of lignocellulosic biomass. For purposes of comparing alternative transportation energy systems, self-consistent analyses were also developed for production from biomass of H_2 (as a fuel cell vehicle fuel) and of electricity (for EVs), drawing from previous Princeton work on these systems. Figure 9 shows schematically the six sets of conversion systems investigated over the course of this project. Counting several permutations of process configurations within each set of conversion systems, a total of 14 process configurations were designed and assessed. Because a primary focus of this research was on gaining insight into the potential for negative emissions, 13 of the 14 configurations include some level of capture of by-product CO_2 for underground storage. Table II lists the 14 process configurations examined and also the estimated technology readiness level (TRL) of each. A summary description and discussion of TRL for each set of conversion systems is given below. Table III summarizes the energy and carbon performance of each process configuration. Full process descriptions and process simulation assumptions and results are given in the cited references.

3.1.1 Gasification - Fischer-Tropsch

Hydrocarbon fuels are produced by gasifying biomass, cleaning the resulting syngas, adjusting its H_2:CO ratio to the optimal value for Fischer-Tropsch (FT) synthesis, removing CO_2 using an absorption process, and then converting the remaining syngas to liquids via FT reactions. The resulting liquid hydrocarbons are upgraded and purified onsite. A total of five variants of gasifer-FT systems were investigated (Table II). Three

variants use indirectly-heated gasification, whereby the combustion of some feedstock to supply heat to drive the gasification reactions occurs in an external vessel, with heat transferred to the gasifier via a solid material (e.g., sand) heated in the combustor [21]. Two variants use directly-heated (partial-oxidation) gasification, with 95% pure O_2 as oxidant rather than air to avoid nitrogen dilution of the syngas [22]. With gasification, co-feeding of a fossil fuel can be accommodated relatively easily – natural gas with indirectly-heated gasification and coal with directly-heated gasification – which in some cases can improve overall economics. A final process-configuration variable is the design of the CO_2 capture system. Directly-heated gasifier systems lend themselves to relatively easy capture of most of the byproduct CO_2, whereas with indirectly-heated gasification a lesser fraction of CO_2 is as readily capturable, and full CO_2 capture requires a more involved and costly design. As indicated by the estimated TRL (Table II), gasification-based hydrocarbon fuels production is a relatively well-developed technology, though there are as yet no commercial biomass-fed systems operating anywhere.

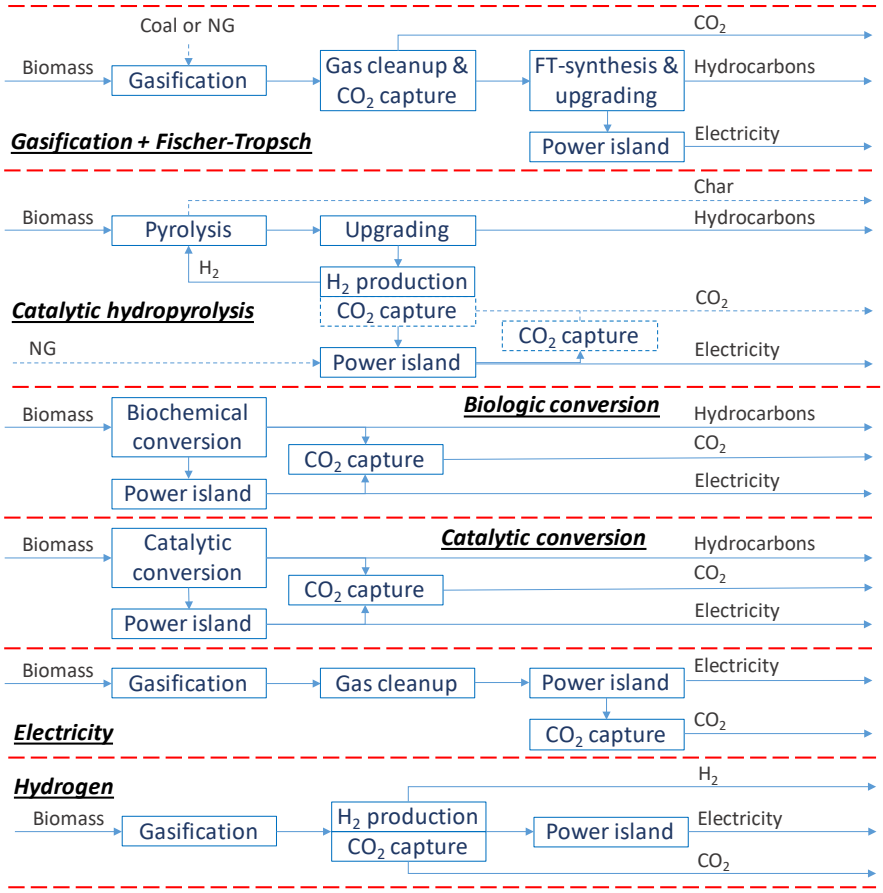

Figure 9. Schematic overview of the different conversion options. The dashed blue lines are option configurations.

Table II Process design variants designed / assessed in this project.

Case #		TRL (*a*)
Indirectly-heated gasification + synthesis → Fischer-Tropsch fuels		**6 – 7**
1	With mild CO_2 capture (IGFT)	
2	With full CO_2 capture (IGFT+)	
3	With mild CO_2 capture + natural gas assist (IGFT-NG)	
Directly-heated gasification + synthesis → Fischer-Tropsch fuels		**6 – 7**
4	With full CO_2 capture + coal assist (DGFT-coal)	
5	With full CO_2 capture (DGFT)	
Catalytic hydropyrolysis + upgrading → hydrocarbon fuels		**4 – 5**
6	Without CO_2 capture (HPyr-V)	
7	With mild CO_2 capture (HPyr-P)	
8	With full CO_2 capture (HPyr-C)	
9	With mild CO_2 capture + natural gas assist (HPyr-P-NG)	
Enzymatic hydrolysis + sugar conversion → hydrocarbon fuels		**1 – 2**
10	Microbial conversion + CO_2 capture (Micro)	
11	Catalytic conversion + CO_2 capture + H_2 from NG (CatNG)	
12	Catalytic conversion + CO_2 capture + H_2 from biomass (CatBio)	
Gasification → Hydrogen, Electricity		**6 – 7**
13	Hydrogen production + CO_2 capture	
14	Electricity production + CO_2 capture	

(a) TRL is Technology Readiness Level, the scale for which ranges from 1 to 9. TRL is an estimate of the maturity of a technology. Different organizations define TRL in somewhat different ways. The TRL estimates in this table are based on guidelines published by the Office of Fossil Energy, US Department of Energy [24]: a TRL of 1 describes the earliest development stage, e.g., proof of scientific concept; a TRL of 9 is assigned to a fully-integrated process that has successfully operated at minimum plausible commercial scale across a full range of expected operating conditions.

3.1.2 Catalytic hydropyrolysis

In this process [23], biomass is heated to around 400°C in a catalytic fluidized bed in a pressurized H_2-atmosphere. The biomass decomposes into char, liquids and vapors. A second catalytic bed upgrades the liquids. Fractional condensation yields hydrocarbon fuels and the non-condensable vapors are used to produce the H_2 required for the process. Waste gases and char are burned to generate process heat, steam and electricity. The raw hydrocarbons require minor additional upgrading at an offsite refinery to be suitable for transportation use. Four variants of the hydropyrolysis process were investigated (Table II): *i)* a case without CO_2 capture; *ii)* a case with mild CO_2 capture via a physical absorption step in the H_2 generation section; *iii)* a case with full CO_2 capture using chemical absorption on the combustor flue gas stream; and *iv)* a case for which char is not burned, but instead used as a soil amendment (thereby sequestering its carbon in the soil). Natural gas is used as a replacement fuel for the char in the latter case and, additionally, a physical absorption of CO_2 is included in the H_2 generation section. This process is assigned a TRL of 4 to 5: it has been demonstrated at bench scale at the Gas Institute of Technology (Chicago) and subsequently was licensed to Shell International, which is constructing (as of early 2018) a pilot-scale demonstration plant in India that will use waste biomass as input.

Table III. Energy, carbon, and economic performance of bioconversion options.

Process (*a*)		**IGFT**			**DGFT**		**HPyro**				**Sugars conversion**			**H_2**	**Elec**
											Micro	CatNG	CatBio		
CO_2 capture system (*b*)		P	C + P	P	P	P	-	P	C	P	C	C	C + P	P	P
Fossil fuel supplement		-	-	NG	Coal	-	-	-	-	NG	-	NG	-	-	-
Energy inputs															
Biomass	MW_{HHV}	449	449	449	711	711	778	778	778	778	425	425	665	983	983
NG	MW_{HHV}			504						110					
Coal	MW_{HHV}				2,281										
Imported elec. (*c*)	MW		19								19	11	11	10	
Imported H_2 (*c*)	MW_{HHV}										9	152			
Energy and non-energy outputs															
Net electricity (*d*)	MW			40			55	48	13	39					418
Net hydrogen (*d*)	MW													526	
Char	t/hr									21					
H_2SO_4	t/hr				22	0									
Captured CO_2	tCO_2/hr	35	84	33	597	149		62	123	62	89	65	72	293	235
Gasoline-like	MW_{LHV}	115	115	247	195	44	297	297	297	297		46	46		
Jet fuel-like	MW_{LHV}				873	196									
Diesel-like	MW_{LHV}	119	119	254			149	149	149	149	128	199	199		
Total efficiency (*e*)	%HHV	56	51	61	38	36	69	68	63	74	28	37	38	62	43
Carbon balance															
INPUT C															
Biomass	kgC/s	11	11	11	19	19	20	20	20	20	10	10	16	25	25
Coal or NG	kgC/s			7	58					2					
OUTPUT C															
Char	kgC/s									4					
Biofuel	kgC/s	4	4	10	20	5	9	9	9	9	3	5	5		
CO_2 for storage	kgC/s	3	6	3	45	11		5	9	5	7	5	10	22	18
Gasifier ash	kgC/s				2										
To atmosphere	kgC/s	4		6	10	3	10	6	1	4	1	1	1	2	7

(a) IGFT = Indirectly heated gasification with Fischer-Tropsch; DGFT = Directly heated gasification with Fischer-Tropsch; HPyro = Catalytic hydropyrolysis; Micro = microbial sugars conversion; CatNG = Catalytic sugars conversion, with required H_2 from NG; CatBio = Catalytic sugars conversion, with required H_2 via biomass gasification; H_2 = Hydrogen production; Elec = Electricity production.

(b) The CO_2 capture system design is with '-' (no capture), 'P' (physical absorption by a solvent), or 'C' (chemical absorption by a solvent).

(c) Purchased quantity, above and beyond what is self-produced and consumed onsite.

(d) Net exports after satisfying onsite requirements.

(e) Ratio (expressed as a percentage) of the sum of energy outputs divided by sum of primary-energy inputs. The ratio of LHV-to-HHV for liquid fuel products is 0.93. For H_2, it is 0.85. For imports of electricity and H_2, the assumed efficiencies of conversion from primary energy are 40% and 70%, respectively.

3.1.3 Microbial conversion of sugars

The microbial conversion pathway relies on first chemically decomposing raw biomass into simple sugars via chemical pretreatment and enzymatic hydrolysis. The resulting sugars are converted via microbial processing into free fatty acids (FFA) that are in turn hydrotreated (via use of a small amount of imported H_2 assumed to be made by steam reforming of natural gas without CO_2 capture) to produce hydrocarbon fuels in the diesel range. The lignin byproduct of the pretreatment and hydrolysis steps is recovered and burned to generate steam and electricity. Remaining organic waste is anaerobically digested into biogas, which is also burned on site to provide process heat and electricity. For our study, we modified a detailed design for this process published by the National Renewable Energy Laboratory (NREL) [25] by integrating capture of CO_2 into the NREL design. The microbial conversion step in the process is still under development at the laboratory scale and the conversion yields assumed in the NREL study have not yet been demonstrated to be achievable in the laboratory. Accordingly, we have assigned this process a TRL of 1 to 2.

3.1.4 Catalytic conversion of sugars

The catalytic sugar conversion process begins with front-end processing of biomass identical to that in the biochemical sugar conversion pathway described above to produce sugars. The sugars are then converted into a mixture of hydrocarbons using a hydrogen-assisted solid-acid catalytic process involving deoxygenation and oligomerization. This is followed by additional hydroprocessing to produce a mix of gasoline to diesel range liquids, with an emphasis on the diesel range. The catalytic process consumes a significant quantity of H_2, but the final liquid product does not need further upgrading. As with the biochemical conversion system described above, the lignin byproduct of the pretreatment and hydrolysis steps is recovered and burned to generate steam and electricity, and other organic waste is anaerobically digested into biogas, which is also burned on site to provide process heat and electricity. Our process design for the catalytic conversion system is based on a detailed NREL study [26]. We modified NREL's design to include capture of CO_2 via chemical absorption from the flue gases generated by the combustion of lignin and biogas. In a second configuration the needed hydrogen is produced onsite via gasification of additional biomass feedstock using a process like that described in the next paragraph. The catalytic conversion step in the process is still under development at the laboratory scale and the conversion yields assumed in the NREL study we used have not yet been demonstrated to be achievable in the laboratory. Like the microbial conversion pathway, we have assigned a TRL of 1 to 2 for this process.

3.1.5 Hydrogen production

The hydrogen production process starts by gasifying biomass in oxygen under pressure in a fluidized-bed reactor, cleaning the resulting synthesis gas, and subjecting it to water-gas shift processing to increase the concentrations of both H_2 and CO_2: ($CO + H_2O \rightarrow H_2 + CO_2$). The CO_2 is then removed using a physical-solvent absorption process, and pure H_2 is produced from the resulting stream via pressure swing adsorption (PSA) by removing non-H_2 components. The PSA off gases are burned in the power island to produce steam and electricity. The process design from earlier Princeton work [27] provided the starting point for the design of the hydrogen production process evaluated here. That original design was modified to include drying and compressing of the removed CO_2 for pipeline transportation to an underground injection/storage site. As

with the other gasification-based conversion processes described above, the technology components for making H_2 from biomass are all relatively well developed, but there are as yet no commercial biomass-H_2 production systems operating anywhere. As a result we have assigned this process a TRL of 6 to 7.

3.1.6 Electricity production

Electricity production from biomass was simulated for a gasification-based system design modified from an earlier Princeton design [28]. The earlier design utilized pressurized, oxygen-blown fluidized-bed gasification, followed by gas cooling to 350°C and filtration at this temperature prior to combustion of the cleaned gas in a gas turbine combined cycle power island. The original study did not include CO_2 capture, so modifications were made to the earlier design to include addition of (a) water-gas shifting (WGS) following the filtration step and (b) gas cooling to ~40°C as needed for (c) CO_2 removal via physical absorption. The captured CO_2 is recovered from the physical-absorption solvent, dried, and compressed for pipeline transportation to an underground injection/storage site. In total, 72% of the carbon input as biomass is captured as CO_2. (Biomass gasification produces some CH_4, which when burned as part of the hydrogen-rich fuel gas sent to the gas turbine, results in CO_2 emissions to the atmosphere.) Like the H_2 production system described above, this electricity process design involves technology components that are relatively well developed, but as yet have not been demonstrated together at any scale. Accordingly, we have assigned a TRL of 6-7 to this process.

3.2 Comparative Analysis of Transportation Pathways

We completed calculations that provide comparative perspectives, in the context of mid-century U.S. transportation energy and GHG emissions, of the different biomass conversion pathways investigated.

3.2.1 Assumptions

For this analysis, we assumed average fuel economies of vehicles using liquid fuel, hydrogen, or electricity (Table IV) and unit GHG emission factors (Table V). For cost comparisons, we developed the capital cost estimates shown in Table VI, representing costs for first-of-a-kind facilities built in the U.S. As commercial deployment proceeds, it is conceivable that costs will be reduced. Capital costs are based on detailed published studies that use varying methodologies, so we have made adjustments to harmonize the cost estimates across the different pathways. Detailed discussion of our capital cost estimates will appear in a forthcoming publication [29]. The other costs shown in Table VI follow from the associated assumptions enumerated in Table VII. Other assumptions in Table VII are used in calculating levelized bioenergy conversion costs.

Table IV. Assumed average fuel economies in 2050 for U.S. light-duty vehicles

Fuel	**Prime mover**	**mpgge** (*a*)	**Miles / MJ**	**km / MJ**
Liquid hydrocarbon	IC engine	60	0.50	0.8
Hydrogen	Fuel cell	90	0.75	1.2
Electricity	Battery	120	1.00	1.6

(a) mpgge = miles / gallon gasoline equivalent. For perspective, under US CAFÉ standards the average fuel economy of new light-duty vehicles in 2025 (largely IC engine vehicles) will be 54.5 mpg [30]; H_2-fuel cell and battery-electric vehicles currently on the market have fuel economies, respectively, of 57 – 68 mpgge (56 – 67 mi/kgH_2) and 72 – 136 mpgge (0.47 – 0.25 kWh/mi) [31].

Table V Input assumptions for lifecycle greenhouse gas emissions analysis.

Greenhouse gas emission factors	Units	Value
Upstream biomass (*a*)	kg CO_{2e} / GJ_{HHV} agro-residue kg CO_{2e} / GJ_{HHV} perennial grasses	9.6 4.5
Upstream natural gas (*b*)	kg CO_{2e} / GJ_{HHV} NG	8.2
Upstream coal (*c*)	kg CO_{2e} / GJ_{HHV} coal	4.93
Grid electricity (*d*)	kg CO_{2e} / MWh	421
CO_2 transport, injection & storage (*e*)	kg CO_{2e} / t CO_2 stored	7.03
Imported hydrogen (*f*)	kg CO_{2e} / kg H_2	11.9
Gasoline-like fuel delivery to user (*g*)	kg CO_{2e} / GJ_{LHV} gasoline	0.91
Jet fuel-like fuel delivery to user (*g*)	kg CO_{2e} / GJ_{LHV} jet fuel	0.84
Diesel-like fuel delivery to user (*g*)	kg CO_{2e} / GJ_{LHV} diesel	0.80
Lifecycle petroleum-derived liquid fuel (*h*)	kg CO_{2e} / GJ_{LHV} HC	90.7
Lifecycle corn ethanol (*i*)	kg CO_{2e} / GJ_{LHV} EtOH	47.2

(a) Source: [32]. These are equivalent GHG emission from fossil-fuel using cultivation, harvesting, and transporting equipment. (The analysis in Section 3.2.3 additionally factors in carbon uptake by soil and N_2O emissions from fertilizer use with production of perennial grasses.).
(b) Estimated emissions for natural gas production and delivery of 2.48 kg $C_{eq.}$/GJ_{LHV} are from [33], and the ratio of HHV to LHV is 1.11.
(c) From Pietro, *et al*. [34] for lignite, as cited by [22].
(d) Our estimate of the lifecycle emissions for a natural gas combined cycle without CCS, based on [35].
(e) Emissions during transport and injection of pressurized CO_2 [36]. Assumed leakage during storage is zero. Transport losses are 0.0081 kg CO_2 lost/(t CO_2 captured * km transported), and 250 km transport is assumed. Injection losses are 5 kg CO_2/t CO_2 delivered.
(f) From [37] for hydrogen via steam reforming of natural gas.
(g) These are the GHG emissions associated with distributing hydrocarbon fuels from the conversion facilities to the end-users. The values are assumed to be the same as given by [38] for petroleum-derived, gasoline, jet fuel, and diesel.
(h) Estimated weighted-average well-to-wheel emissions for gasoline, jet fuel and diesel produced in the U.S. in 2005 [38].
(i) From ICF [39].

Table VI. Cost estimates for the investigated pathways.

Process		IGFT			DGFT		HPyro				Sugars conversion			H_2	Elec
											Micro	CatNG	CatBio		
CO_2 capture system		P	C + P	P	P	P	-	P	C	P	C	C	C + P	P	P
Fossil fuel supplement		-	-	NG	Coal	-	-	-	-	NG	-	NG	-	-	-
Costs (2015 dollars), for plant scale of 500 MW_{HHV} biomass input															
Capital cost (*a*)	$10^6$$	874	1,038	1,327	5,022	1,587	330	408	519	401	1,077	1,142	1,320	732	980
O&M cost (*b*)	10^6 $/yr	35	42	53	201	63	18	21	26	21	50	58	65	29	39
Refining (*c*)	10^6 $/yr	26	26	26	31	7	57	57	57	57	-	-	-	-	-
CO_2 storage (*d*)	10^6 $/yr	14	21	14	58	27	-	18	25	18	21	18	19	38	34

(a) Total estimated overnight capital cost for first-of-a-kind facilities.
(b) Includes standard (rule-of-thumb) O&M costs (Table VII) plus expensive consumables that fall outside the rule-of-thumb calculation, e.g., hydropyrolysis catalysts and H_2SO_4.
(c) Some additional refining is required with most of the processes for the products to meet fuel specifications.
(d) Cost estimate includes pipeline transport, injection into saline aquifers, and long-term monitoring.

Table VII Key assumptions for cost analyses.

Parameter	Units	Value
Annual capital charge rate	1/year	0.16
Standard annual (non-feedstock) O&M costs (a)	% of overnight capital cost	4
Delivered biomass feedstock price (b)	\$2015 / GJ_{HHV} biomass	5
Delivered natural gas price (b,c)	\$2015 / GJ_{HHV} NG	5.5
Delivered coal price (b)	\$2015 / GJ_{HHV} coal	2.1
Delivered hydrogen price (d)	\$2015 / GJ_{HHV} H_2	11.8
Electricity sale or purchase price	\$2015 / MWh	70
Crude oil price	\$2015 / bbl	80
Refining cost for gasoline-like fuels (e)	\$2015 / GJ_{LHV} gasoline	5.59
Refining cost for diesel-like fuels (e)	\$2015 / GJ_{LHV} diesel	2.34
CO2 transport and injection (f)	\$2015 / t CO_2 stored	12-53
Annual operating time (g)	hours/year	7,889

(a) In the case of the hydropyrolysis facilities, the total O&M costs includes this standard O&M cost plus the cost the specialty hydropyrolysis catalyst. According to Tan [40], 52.89 lb/hr of makeup catalyst are required for a 2,000 metric t_{dry}/d biomass input design (equivalent to 0.288 kg catalyst/t_{dry} biomass). Tan's catalyst price is 14,000 $\$_{2007}$/short ton (equivalent to 16.4 $\$_{2015}$/kg catalyst), or 4.7 $\$_{2015}$ per t_{dry} biomass.

(b) Assumed 20-year levelized price.

(c) This is the levelized U.S. natural gas price for industrial users in the Reference case of the USDOE Annual Energy Outlook 2016 for the period 2020–2040 [41].

(d) The H_2 price is estimated for steam methane reforming of natural gas using the following equation [42]: H_2 price (\$/kg) = 0.768 + [0.165 * NG price], where NG price is in $\$/GJ_{HHV}$. The higher heating value of H_2 is 141.8 MJ/kg H_2.

(e) These are based on petroleum-refiner margins of 0.67 \$/gallon gasoline and 0.32 \$/gallon diesel, as estimated from EIA AEO 2016 Reference Scenario [43]. These are levelized values (7% discount rate) of the difference annually between the average U.S. refiner's acquisition cost of imported crude oil and the average U.S. wholesale price of gasoline (or diesel) projected for the period 2021-2040.

(f) Costs in $\$/tCO_2$ are from [22]: Transport cost = 6.432 x $(tCO_2/d\ transported)^{-0.65}$ x $(km\ transported)^{1.13}$; Injection cost = 5 $\$/tCO_2$ (fixed).

(g) This corresponds to a 90% annual capacity factor.

3.2.2 Results

Several metrics were calculated for each of the 14 processes analyzed. A first comparative metric is shown in Figure 10: the transportation services (vehicle-km) that could be delivered per unit of biomass feedstock via different pathways. The two highest cases (#3 and #4) are for fuel production that includes co-processing considerable amounts of natural gas or coal. A trade-off in these cases is higher greenhouse gas (GHG) emissions, as discussed below. For designs that process exclusively biomass to make liquid fuels, designs based on catalytic hydropyrolysis (#6 - #8) give the highest vehicle-km per unit of biomass because of the high yield of liquid fuels for this process compared with the other processes. Among all biomass-only systems, the hydrogen and electricity pathways provide the highest vehicle-km per GJ biomass due primarily to the higher fuel economy for the vehicles that use these fuels (Table IV).

Figure 11 shows another metric, lifecycle GHG emissions per 100 vehicle-km, for the 14 pathways. The emissions estimates include those for growing, harvesting, transporting, and converting the biomass to fuel, as well as emissions from fuel use. The biomass feedstock assumed for Figure 11 has upstream emissions corresponding to those

shown in Table V for perennial grasses and excludes consideration of soil carbon uptake or release. For all systems except #6 (which includes no CO_2 capture), some CO_2 of biogenic origin is captured at the conversion plant and permanently sequestered underground, thereby contributing a negative component to the full fuel-cycle emissions.

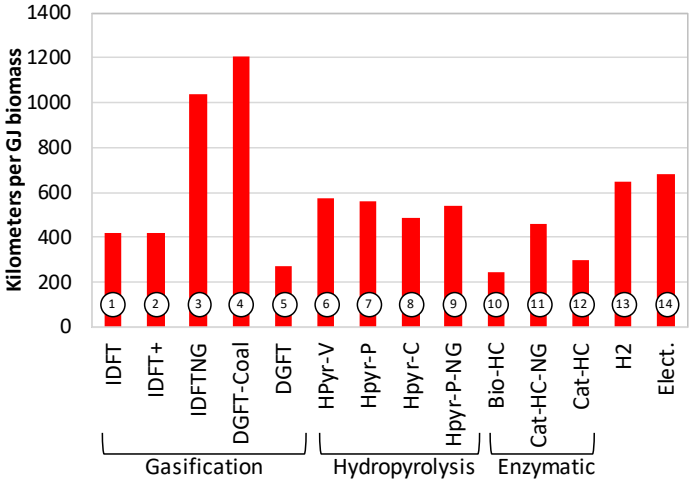

Figure 10. Vehicle-kilometers driven per unit of biomass input with different conversion processes. Circled numbers correspond to case numbers in Table II.

For all 14 systems net emissions are well below those of petroleum-derived fuels. The net emissions are negative for all except cases #3, #4, and #6. Cases #3 and #4 co-process substantial amounts of fossil fuels. Case #6 does not use CO_2 capture and storage. The three cases with the most-negative emissions, #5, #10 and #12, correspond to those with the lowest transportation fuel yields (Figure 10). For these cases, the share of the carbon in the biomass feedstock that ends up in the liquid fuel is lower than in other systems, allowing a larger share of the biomass carbon to be captured and sequestered and thus giving more negative emissions per vehicle-kilometer.

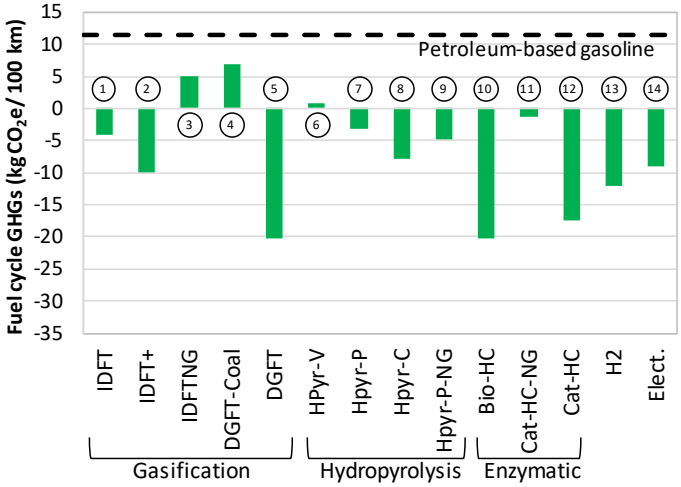

Figure 11. Fuel cycle greenhouse gas emissions per 100 vehicle-kilometers with different conversion processes. These results incorporate GHG emissions factors shown in Table V, including upstream biomass emissions of 4.5 $kgCO_{2e}/GJ_{biomassHHV}$. These calculations assume zero net exchange of GHGs between soil and atmosphere. Circled numbers correspond to case numbers in Table II.

Figure 12 compares levelized costs of production for all 14 pathways, assuming the GHG emissions price is zero (left graph) or \$100/tCO_{2e} (right graph). The cost of gasoline from \$80/bbl crude oil is shown for comparison. With no GHG emissions price, only the hydropyrolysis system with venting of CO_2 is competitive with gasoline, but all of the hydropyrolysis cases and the hydrogen case are only modestly more costly than gasoline. In the presence of a \$100/tCO_{2e} GHG emissions price, the cost of all the biofuel options improves relative to gasoline, as expected. Among the biofuel options, the hydropyrolysis, hydrogen, and electricity systems are all clearly competitive with gasoline, while the remaining biofuel options are still considerably more costly.

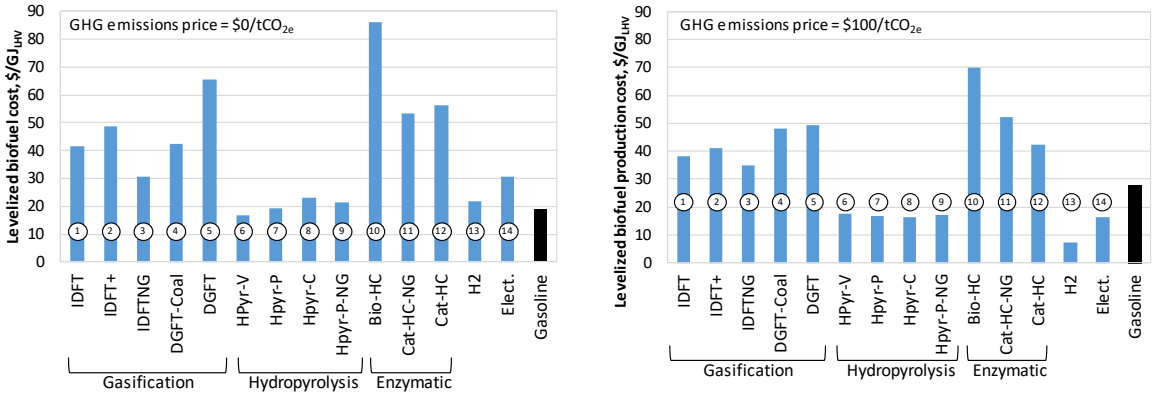

Figure 12. Levelized-cost of biofuels (liquids, hydrogen, and electricity), with zero GHG emissions price (left) and \$100/tCO_{2e} (right). Costs for gasoline from \$80/bbl crude oil are also shown. Circled numbers correspond to case numbers in Table II.

Figure 13 combines the fuel economy of vehicles (Table IV) with the levelized biofuel production costs in Figure 12 to estimate the driving cost per km. The ranking against gasoline of the driving cost for liquid biofuel systems is unchanged from the ranking of levelized fuel production costs in Figure 12, with or without a GHG emissions price. However, the higher efficiency of hydrogen- and electricity-powered vehicles relative to liquid fueled vehicles leads to both of these biofuel systems having lower driving costs than for gasoline, even in the absence of a GHG emissions price. The competitiveness of all biofuel options increases in the presence of a GHG emissions price (Figure 13, right).

3.2.3 A Thought Exercise for Mid-Century

As a thought exercise, we coupled results from the above analysis of biomass processing options with projections of potential biomass feedstock supplies in 2050 to assess the extent to which bioenergy might help meet mid-century U.S. transportation energy needs and GHG mitigation goals. Potential biomass feedstock supplies in 2050 were quantified with the aims of minimizing land-competition with food production and minimizing indirect land-use change emissions. We estimated production of the two largest residues of food crop production in the U.S., as well as perennial grasses grown on abandoned agricultural land, as estimated by CSU colleagues.

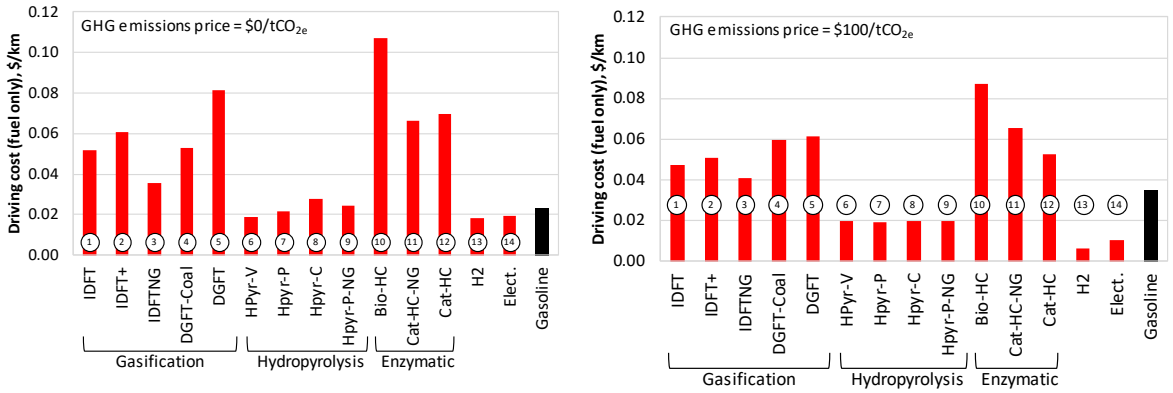

Figure 13. Driving cost (fuel only) with biofuels (liquids, hydrogen, and electricity), with zero GHG emissions price (left) and $100/tCO$_{2e}$ (right). Driving cost with gasoline (for $80/bbl crude oil price) is also shown. Circled numbers correspond to case numbers in Table II.

The projected availability in 2050 of corn and wheat residues, which account for the majority of all agricultural residues generated in the U.S., were aggregated from county-level estimates in the US DOE *Billion Ton Study* [44] and totaled 147 million tonnes (Figure 14), or about 2.6 EJ, of which 2.0 EJ are corn stover. That study estimates these quantities of residues can be collected without long-term reductions in soil organic carbon and delivered to farm gates for $55 or less per dry tonne for corn stover (or 3.0 $/GJ$_{HHV}$) and $66 or less per dry tonne for wheat straw (or 3.7 $/GJ$_{HHV}$).

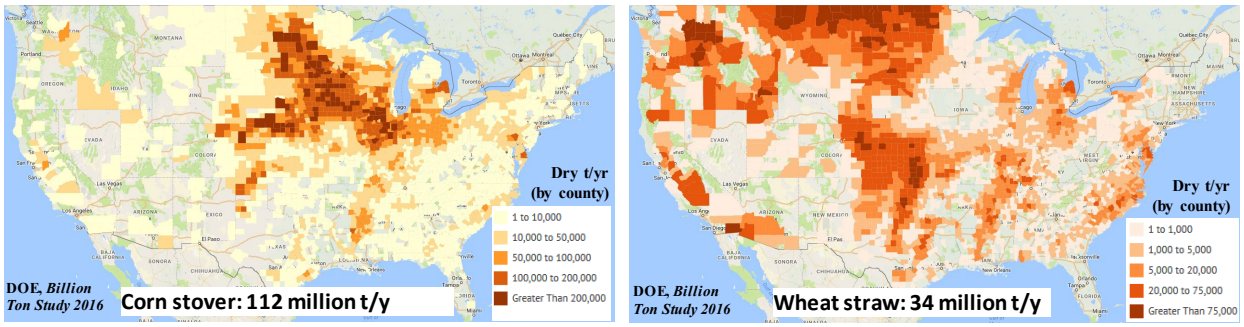

Figure 14. Corn and wheat residues assumed to be available in 2050 as energy feedstock for biomass-based transportation energy production.

The CSU estimates of perennial grasses grown on abandoned cropland across the Eastern U.S. ranges from 281 to 492 million t/y (Table I), or 5.1 to 8.8 EJ/y. Thus, the total lignocellulosic biomass supply in 2050 in our thought exercise is 7.7 to 11.5 EJ/y.

To help put these numbers in some perspective, we examined projected transportation energy demands in 2050 in the IEA's 2°C scenario (2DS) – designed to limit global warming to no more than 2°C above the pre-industrial level (Table VIII). Considering that total 2DS transportation energy demand in the U.S. (14.1 EJ) is well above our estimate of biomass feedstock availability, our biofuels would provide only a portion of U.S. transportation energy needs. If GHG emissions mitigation goals consistent with a

2DS scenario are to be met, there would likely need to be aggressive electrification of transportation, together with decarbonization of the grid. With this in mind, if all non-air passenger travel were to be electrified (using zero-GHG electricity), as well as light road freight, the remaining liquid hydrocarbon fuel requirements in 2050 would be 8.4 EJ (red values in Table VIII).

Table VIII. U.S. transportation energy demands in 2050 for 2DS. The red values (totaling 8.4 EJ) are assumed to require liquid hydrocarbon fuels. The others are assumed to be able to use zero-GHG electricity.

	Passenger (EJ)	**Freight (EJ)**	**Total (EJ)**
Air	2.67	0.00	2.67
Light road	4.36	0.88	5.24
Heavy road	0.40	4.25	4.65
Rail	0.11	0.51	0.62
Shipping	0.00	0.98	0.98
Totals	**7.53**	**6.61**	**14.14**

(a) Source: IEA [45].

Figure 15 shows net GHG emissions from the transportation sector using 8.4 EJ of liquid hydrocarbon fuels, with petroleum fuels supplementing the amount of biofuel that could be produced from 7.7 EJ of biomass (left side of figure) or 11.5 EJ of biomass (right side of figure). Only the seven bioconversion pathways in Table II that utilize solely biomass as input and produce liquid hydrocarbon fuels are shown. For each route, emissions are estimated without CO_2 capture (left bar of each pair) and with CO_2 capture (right bar). The difference in net emissions with and without CCS for a given bioconversion route is the amount of geologic CO_2 that would need to be stored in the case with CCS. In Figure 15, the storage required ranges from a low of about 170 million tCO_2/yr (cases 1,7) to a high of between 400 and 450 million tCO_2/y (cases 2,5,10,12) in the left panel and from about 250 million tCO_2/yr (cases 1,7) to between 600 and 665 million tCO_2/y (cases 2,5,10,12) in the right panel. Shown for reference in Figure 15 is a 2050 decarbonization target for the transportation sector that is notionally consistent with the U.S. contributing its share to achieving a 2°C cap in global warming (80% below 2005 emissions).

In the case with lower biomass supplies (left panel), when CCS is included with bioconversion all of the pathways are able to achieve emissions well below the 2050 target. Without CCS four of the pathways (#1, 2, 7, and 8) are still able to just meet the target. In the case with higher total biomass availability (right panel), the same four cases reduce emissions well below the target, even without CCS included. With CCS included, all seven pathways produce emissions well below the target, and five of them deliver significant net negative emissions (200 to 300 million tCO_2/y).

3.3 Examining prospective pace of commercial deployments

Our results above suggest that U.S. transportation energy and GHG emissions targets for a 2DS scenario in 2050 may be met via aggressive electrification of transportation, decarbonization of electricity supply, and deployment of liquid fuels from sustainably

produced biomass. An important question is whether such a biofuels industry could develop fast enough to achieve the 2050 deployment level in our thought exercise.

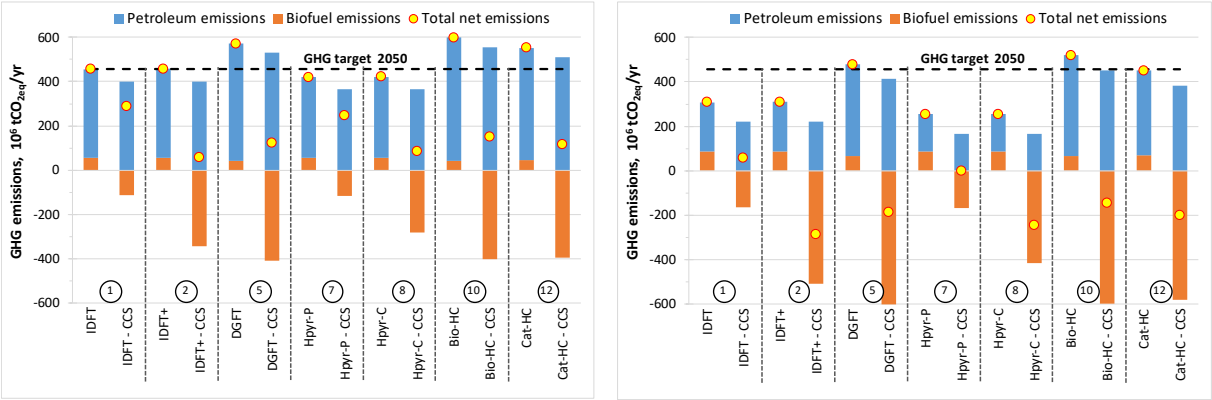

Figure 15. U.S. net GHG emission from transportation in 2050 for the thought exercise described in the text. The left and right graphs assume a total of biomass feedstock supply of 7.7 EJ and 11.5 EJ, respectively. Net soil carbon emissions are as in Table I. Circled numbers correspond to case numbers in Table II.

We explore this question by examining different scale-up rates for an advanced biofuel production industry and the resulting contributions that advanced biofuels might make by mid-century. We compare scale-up rates with the most relevant historical precedent, the expansion of the US corn-ethanol industry. That industry initially grew slowly, starting in the early 1980s, for about 3 decades, but more rapidly once significant incentives were introduced beginning in 1999 when California banned MTBE as a gasoline oxygenate, spurring increased demand for ethanol as a substitute (Figure 16). Additional incentives followed, further accelerating growth, but growth subsequently slowed as total output approached the corn-ethanol supply limit under the Renewable Fuel Standard (RFS-2) legislation.

The curve fit to the data in Figure 16 derives from the following equation:

$$P_t = C_1 \cdot (t - t_0) + \frac{C_2}{1+e^{-b\cdot(t-t_{infl})}} \qquad (1)$$

Where P_t is petajoules of feedstock processed in year t. Time zero (t_0) is 1981, representing the start of the corn-ethanol industry. C_1, C_2, b, and t_{infl} are constants that have been tuned to achieve a visual best fit. In Figure 16, C_1 = 12.6/year, C_2 = 1680 PJ/year, t_{infl} = 2009.5, and b = 0.6/year.

Eqn. 1 is a modified logistics function. (A pure logistics function includes only the second term on the right.) Logistics functions are used to describe growth processes (e.g., population expansion or infectious disease spread) that begin slowly, then accelerate exponentially before decelerating and eventually reach a saturation level.

We explore logistics functions of the same form as Eqn. 1 to represent the scale-up trajectory of a future advanced lignocellulosic biofuels industry. There is next-to-no commercial production of lignocellulosic biofuels today largely because the technologies have not yet matured to the point where they can be deployed commercially, even if government incentives are available. However, for this thought exercise, we will assume that R&D progresses rapidly enough that technologies are ready for commercial

deployment beginning in 2025 and that government incentives in place at that time will be sufficient to motivate commercial deployment. We also assume that commercial biofuel production begins in 2025 with enough biomass processed to produce 500 million gallons of biofuel, or 65 PJ_{HHV} of biofuel, assuming the energy content of the biofuel is similar to that of gasoline. (For comparison, the average US corn-ethanol facility today has a production capacity of 78 million gallons per year, or 7 PJ_{HHV}, and the largest one has a capacity of 375 million gallons per year, or 33 PJ_{HHV}.)

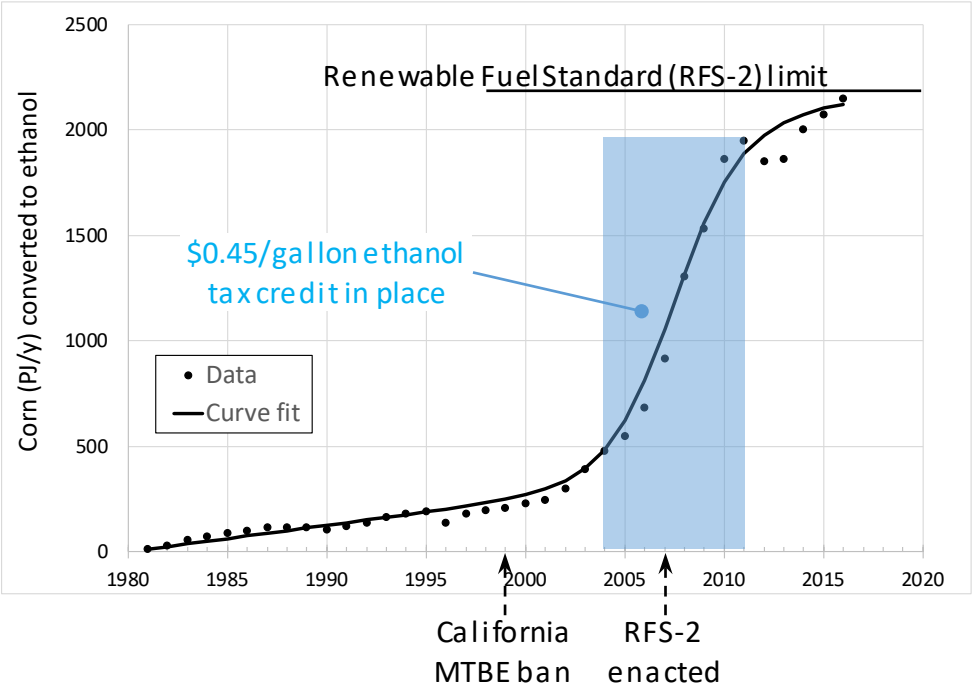

Figure 16. Historical growth of US corn-ethanol industry (corn energy input basis) and incentives that have driven it.

If growth of an advanced biofuel industry from 2025 follows a trajectory like that seen for corn ethanol, i.e., slow linear growth for about 20 years before accelerating, the output of a lignocellulosic bioconversion industry by 2050 would still be only a fraction of that of the current corn-ethanol industry.

Alternatively, if sufficient incentives were in place by 2025 so that investment in the industry accelerates without the slow initial phase, growth trajectories like those in Figure 17 could result. The solid lines shown there follow Eqn. 1, but without the linear term (i.e., $C_1 = 0$). The value of C_2 is 7,700 PJ/y (left panel) and 11,500 PJ/y (right panel), covering the range of sustainable biomass supplies estimated above. The value of t_{infl} varies from one line to the next, representing different industry expansion rates, and for each value of t_{infl}, b is set such that the amount of biomass processed in 2025 corresponds to the production of 500 million gallons of biofuel. The dashed lines plot the slopes of the solid lines, i.e., the dashed lines show annual growth rates.

Table IX compares metrics derived from Figure 16 for the US corn-ethanol industry and from Figure 17 for (prospective) advanced biofuel industries. The corn-ethanol

industry grew (in terms of feedstock-energy inputs) from 10% to 90% of the RFS-imposed maximum in the course of 17 years. If an advanced biofuel industry were to grow from 10% to 90% of the target total biomass feedstock-energy input (7.7 EJ or 11.5 EJ) in the same 17 years, the annual average growth in feedstock-energy input during that period would be 3.5 times that of the corn ethanol industry (for the 7.7 EJ target) to 5.7 times (for the 11.5 EJ target). If the advanced biofuel industry were to take longer to reach the 90% threshold, the annual average growth rates would be lower, but still multiples of the growth observed for the corn ethanol industry.

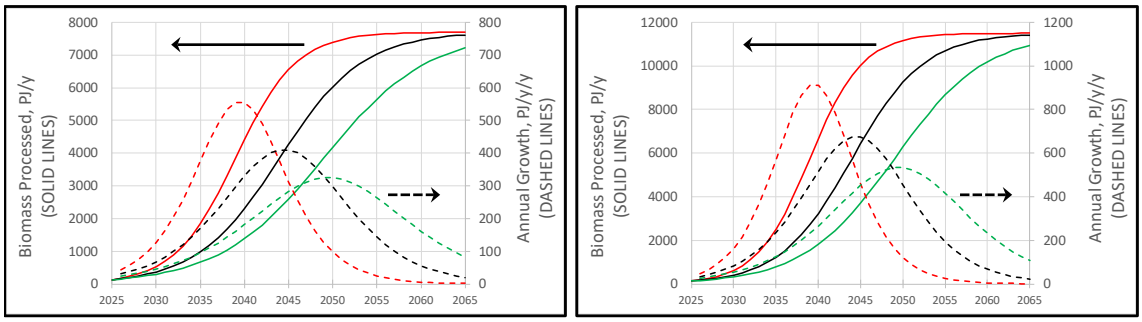

Figure 17. Alternative scenarios for growth of advanced lignocellulosic biofuel industries (biomass input energy basis) starting in 2025. Dashed lines are annual expansion rates (right axis) corresponding to the solid curves of the same color showing annual biomass processed (left axis). The left panel assumes the industry grows ultimately to process 7.7 EJ/y of biomass and right panel assumes 11.5 EJ/y.

Table IX. Comparison of historical US corn-ethanol industry and a prospective advanced biofuel industry.

	Corn ethanol	**Lignocellulosic biofuel industry**					
TARGET feedstock input, EJ/y	2.2	7.7			11.5		
Year 90% of TARGET reached	2012	2046	2054	2062	2046	2053	2061
# of years, 10% to 90%	17	17	23	27	17	23	27
Energy growth, PJ/y/y (a)	111	392	296	232	637	488	378
Volume growth, $Mm^3/y/y$ (a)	10	176	133	104	286	219	169

(a) Average annual expansion rates for feedstock energy or volume during scale-up from 10% to 90% of target feedstock input.

Table IX also shows average annual growth rates expressed in terms of biomass feedstock volumes rather than energy, which reflect the scale of the biomass feedstock supply industry (as distinct from the scale of the biomass conversion industry). For the advanced biofuel industry to achieve the 90% threshold in 17 years, the average annual growth in biomass volume handled would be 18 times the average growth rate observed for the corn ethanol industry with a 7.7 EJ/yr biomass feedstock target. It would be 29 times as large with the 11.5 EJ/y target. The volume growth rates are so much larger for the lignocellulosic bioconversion industry both because of the larger target scales and because the volumetric energy density of baled crop residues or grasses, which constitute the lignocellulosic biomass supply, is only about one-fifth of that for corn grain. At the

target lignocellulosic biomass supply levels, 7.7 and 11.5 EJ/yr, the biomass collection and transport infrastructure would be handling, respectively, 18 and 27 times the volume managed today by the corn-handling infrastructure for the ethanol industry.

In summary, deploying liquid fuels made from sustainably produced biomass feedstocks in the U.S. could help meet a 2050 U.S. GHG emissions target consistent with meeting goals of the Paris Climate agreement. Meeting the target would require using such biofuels only for difficult-to-electrify transportation needs – air and heavy-road, rail, and water-borne freight – and electrifying all non-air passenger and all light-road freight transport using decarbonized electricity. Some biofuel pathways that include CO_2 capture and storage would enable the transportation sector to have net negative emissions.

For an advanced biofuels industry to grow to meet a 2050 2DS target, commercial deployment would need to begin soon. The higher-TRL systems investigated here have the potential to be commercially ready by 2025 with adequate support for research, development, and demonstrations. However, government incentives stronger than those that drove the expansion of the U.S. corn-ethanol industry will be needed to drive commercial buildout of a lignocellulosic biofuels industry at the pace and scale needed to achieve the 2050 GHG emissions target.

Publications

1. A.K. Hailey, J.C. Meerman, E.D. Larson, and Y.-L. Loo, "Low-carbon 'drop-in replacement' transportation fuels from non-food biomass and natural gas," *Applied Energy*, 183: 1722-1730, 2016. http://dx.doi.org/10.1016/j.apenergy.2016.09.068.
2. J.C. Meerman and E.D. Larson, "Negative-carbon drop-in transport fuels produced via catalytic hydropyrolysis of woody biomass with CO_2 capture and storage," *Sustainable Energy and Fuels*, published online April 6, 2017. http://doi.org/10.1039/c7se00013h.
3. Nguyen, F., *A Techno-Economic Analysis of Solid Acid Mechanocatalysis for Biomass Solubilization in the Production of Cellulosic Ethanol*," senior thesis, Chemical and Biological Engineering Dept., Princeton University, 1 May 2017.
4. Lowe, C., *Fermentation by the Non-Oxidative Glycolysis Pathway: a Techno-Economic Analysis*," senior thesis, Chemical and Biological Engineering Dept., Princeton University, 1 May 2017.
5. Yang, Y., Tilman, D., Lehman, C. and Trost, J.J., "Sustainable intensification of high-diversity biomass production for optimal biofuel benefits," *Nature Sustainability*, 1: 686–692, 2018. https://doi.org/10.1038/s41893-018-0166-1
6. Yang, Y. Tilman, D. Furey, G. and Lehman, C., "Carbon storage accelerated by restoration of grassland biodiversity," revised and resubmitted to *Nature Communications*, 2018.

References

1. IPCC, *Climate Change 2014: Mitigation of Climate Change. Contribution of Working Group III to the Fifth Assessment Report of the Intergovernmental Panel on Climate Change* [Edenhofer, O., R. Pichs-Madruga, Y. Sokona, E. Farahani, S. Kadner, K. Seyboth, A. Adler, I. Baum, S. Brunner, P. Eickemeier, B. Kriemann, J. Savolainen, S. Schlömer, C. von Stechow, T. Zwickel and J.C. Minx (eds.)], Cambridge University Press, Cambridge, UK and New York, NY, USA, 2014.
2. IPCC, *Special Report on Global Warming of 1.5°C*, 2018. http://www.ipcc.ch/report/sr15/

3. Larson, E.D., Lehman, C., Tilman, D., and Williams, R.H. (Principal Investigators), "Sustainable Transportation Energy with Net Negative Greenhouse Gas Emissions: an integrated ecological and engineering systems analysis," Research progress report to Stanford University, Global Climate and Energy Project, 9 May 2016.
4. Larson, E.D., Lehman, C., Tilman, D., and Williams, R.H. (Principal Investigators), "Sustainable Transportation Energy with Net Negative Greenhouse Gas Emissions: an integrated ecological and engineering systems analysis," Research progress report to Stanford University, Global Climate and Energy Project, 9 May 2017.
5. Yang, Y., Tilman, D., Furey, G., and Lehman, C., "Carbon storage accelerated by restoration of grassland biodiversity," manuscript revised and resubmitted, *Nature Communications*, 2018.
6. Yang, Y., Tilman, D., Lehman, C. and Trost, J.J., "Sustainable intensification of high-diversity biomass production for optimal biofuel benefits," *Nature Sustainability*, 1: 686–692, 2018.
7. Yang, Y., Tilman, D., Furey, G., Lehman, C., and Smith, T. "Climate benefits of high plant diversity in C4 perennial grasses grown on marginal soils for bioenergy," manuscript in preparation, 2018.
8. Yang, Y. and Jungers, J., "Plant diversity increases yield and stability of bioenergy perennial feedstocks across space," manuscript in preparation, 2018.
9. Field, J. L., Evans, S. G., Marx, E., Easter, M., Adler, P. R., Dinh, T., Willson, B., and Paustian, K. (2018). High-resolution techno–ecological modelling of a bioenergy landscape to identify climate mitigation opportunities in cellulosic ethanol production. *Nature Energy*, *3*, 211–219.
10. Parton, W. J., Schimel, D. S., Cole, C. V., & Ojima, D. S. (1987). Analysis of factors controlling soil organic matter levels in Great Plains grasslands. *Soil Science Society of America Journal*, *51*(5), 1173–1179.
11. Campbell, E. E., Field, J. L., & Paustian, K. (2018). Modelling soil organic matter dynamics as a soil health indicator. In D. Reicosky (Ed.), *Managing soil health for sustainable agriculture* (Vol. Volume 2: Monitoring and management). Cambridge, UK: Burleigh Dodds Science Publishing.
12. Parton, William J., Hartman, M., Ojima, D., & Schimel, D. (1998). DAYCENT and its land surface submodel: description and testing. *Global and Planetary Change*, *19*(1), 35–48.
13. Lewis, S., & Kelly, M. (2014). Mapping the Potential for Biofuel Production on Marginal Lands: Differences in Definitions, Data and Models across Scales. *ISPRS International Journal of Geo-Information*, *3*(2), 430–459.
14. Zumkehr, A., & Campbell, J. E. (2013). Historical U.S. Cropland Areas and the Potential for Bioenergy Production on Abandoned Croplands. *Environmental Science & Technology*, *47*(8), 3840–3847.
15. Field, J. L., Marx, E., Easter, M., Adler, P. R., & Paustian, K. (2016). Ecosystem model parameterization and adaptation for sustainable cellulosic biofuel landscape design. *GCB Bioenergy*, *8*(6), 1106–1123.
16. Homer, C., Dewitz, J., Yang, L., Jin, S., Danielson, P., Xian, G., … Megown, K. (2015). Completion of the 2011 National Land Cover Database for the conterminous United States–representing a decade of land cover change information. *Photogrammetric Engineering & Remote Sensing*, *81*(5), 345–354.
17. US EPA. (2018). Chapter 6: Land Use, Land-Use Change, and Forestry. In *Draft Inventory of U.S. Greenhouse Gas Emissions and Sinks: 1990-2016*.
18. Myhre, G., Shindell, D., Bréon, F.-M., Collins, W., Fuglestvedt, J., Huang, J., … Zhang, H. (2013). Anthropogenic and Natural Radiative Forcing. In T. F. Stocker, D. Qin, G.-K. Plattner, M. Tignor, S. K. Allen, J. Boschung, … P. M. Midgley (Eds.), *Climate Change 2013: The Physical Science Basis. Contribution of Working Group I to the Fifth Assessment Report of the*

Intergovernmental Panel on Climate Change. Cambridge, United Kingdom and New York, NY, USA: Cambridge University Press.

19. Lee, D. K., Aberle, E., Anderson, E. K., Anderson, W., Baldwin, B. S., Baltensperger, D., … Owens, V. (2018). Biomass production of herbaceous energy crops in the United States: field trial results and yield potential maps from the multiyear regional feedstock partnership. *GCB Bioenergy*.
20. Daly, C., Halbleib, M. D., Hannaway, D. B., & Eaton, L. M. (2018). Environmental limitation mapping of potential biomass resources across the conterminous United States. *GCB Bioenergy*, n/a-n/a.
21. Hailey, A.K., Meerman, J.C., Larson, E.D., Loo, Y.L., "Low-carbon 'drop-in replacement' transportation fuels from non-food biomass and natural gas," *Applied Energy*, 183: 1722-30, 2016.
22. Greig, C., Kreutz, T.G., Larson, E.D., Meerman, J.C., and Williams, R.H., *Lignite-plus-Biomass to Synthetic Jet Fuel with CO_2 Capture and Storage: Design, Cost, and Greenhouse Gas Emissions Analysis for a Near-Term First-of-a-Kind Demonstration Project and Prospective Future Commercial Plants*, final report under contract DE-FE0023697 to the National Energy Technology Laboratory, US Department of Energy, 1 September 2017.
23. Meerman, J.C. and Larson, E.D., "Negative-carbon drop-in transport fuels produced via catalytic hydropyrolysis of woody biomass with CO_2 capture and storage," *Sustainable Energy & Fuels*, 1: 866-81, 2017.
24. Office of Fossil Energy, "2014 Technology Readiness Assessment – Overview," Clean Coal Research Program, USDOE, January 2015.
25. Davis, R. Tao, L., Tan, E.C.D., Biddy, M.J., Beckham, G.T., Scarlata, C., Jacobson, J., Cafferty, K., Ross, J. Lukas, J. Knorr, D. and Schoen, P., *Process Design and Economics for the Conversion of Lignocellulosic Biomass to Hydrocarbons: Dilute-Acid and Enzymatic Deconstruction of Biomass to Sugars and Biological Conversion of Sugars to Hydrocarbons*, National Renewable Energy Laboratory, NREL/TP-5100-60223, October 2013.
26. Davis, R. Tao, L., Scarlata, C., Tan, E.C.D., Ross, J., Lukas, J., and Sexton, D., *Process Design and Economics for the Conversion of Lignocellulosic Biomass to Hydrocarbons: Dilute-Acid and Enzymatic Deconstruction of Biomass to Sugars and Catalytic Conversion of Sugars to Hydrocarbons*, NREL/TP-5100-62498, National Renewable Energy Laboratory, March 2015.
27. Larson, E.D., Jin, H., and Celik, F.E., "Large-Scale Gasification-Based Co-Production of Fuels and Electricity from Switchgrass," *Biofuels, Bioproducts, and Biorefining*, 3(2): 174-194, 2009.
28. Jin, H., Larson, E.D., Celik, F.E., "Performance and cost analysis of future, commercially mature gasification-based electric power generation from switchgrass," *Biofuels, Bioproducts, and Biorefining*, 3(2): 142-173, 2009.
29. Meerman, J.C. and Larson, E.D., "A comparative analysis of biofuel conversion options for the United States," (*working title*), manuscript in preparation, December 2018.
30. US Environmental Protection Agency, 40 CFR Part 85, 86 and 600.
31. US Department of Energy, https//www.fueleconomy.org, accessed 17 Dec 2018.
32. Larson, E.D., Fiorese, G., Liu, G. Williams, R.H., Kreutz, T.G. and Consonni, S., "Co-Production of Decarbonized Synfuels and Electricity from Coal + Biomass: An Illinois Case Study," *Energy and Environmental Science*, 3(1): 28-42, 2010.
33. Argonne National Laboratory, The Greenhouse gases, Regulated Emissions, and Energy use in Transportation (GREET) Model, https://greet.es.anl.gov/.
34. Pietro et al., "Life Cycle Analysis of Coal and Natural Gas-fired Power Plants," presented at EPRI Coal Fleet, 20 July 2010.

35. National Energy Technology Laboratory, *Cost and performance baseline for fossil energy plants, Volume 1, revision 2a*, 2013.

36. The Aviation Fuel Life Cycle Assessment Working Group (T.J. Skone, D.T. Allen, C. Allport, K. Atkins, D. Baniszewski, D.G. Choi, et al.), *Life Cycle Greenhouse Gas Analysis of Advanced Jet Propulsion Fuels: Fischer-Tropsch Based SPK-1 Case Study*, AFRL-RZ-WP-TR-2011-2138, Air Force Research Lab, Propulsion Directorate, Wright-Patterson Air Force Base, Ohio, September 2011.

37. Spath, P.L. and Mann, M.K., *Life Cycle Assessment of Hydrogen Production via Natural Gas Steam Reforming*, NREL/TP-570-27637, National Renewable Energy Laboratory, 2001.

38. Skone, T. and Gerdes, K., *Development of Baseline Data and Analysis of Life Cycle Greenhouse Gas Emissions of Petroleum-Based Fuels*, (and companion spreadsheet model, 2009), DOE/NETL-2009/1346, National Energy Technology Lab, 26 November 2008.

39. ICF, A Life-Cycle Analysis of the Greenhouse Gas Emissions of Corn-Based Ethanol, preapred for the US Department of Agriculture, January 2017.

40 E. Tan, Techno-Economic Analysis of the Integrated Hydropyrolysis and Hydroconversion Process for the Production of Gasoline and Diesel Fuels from Biomass, National Renewable Energy Laboratory, 2011.

41. Energy Information Administration, *Annual Energy Outlook 2017*, USDOE.

42. Dillich, S., Ramsden, T., and Melaina, M., "Hydrogen Production Cost Using Low-Cost Natural Gas," DOE Hydrogen and Fuel Cells Program Record 12024, 19 September 2012.

43. Conti, J. Holtberg, P., Diefenderfer, J., Larose, A., Turnure, J. and Westfall, L., *Annual Energy Outlook 2016 – with projections to 2040*, U.S. Energy Information Administration, DOE/EIA-0383(2016), August 2016.

44. Langholtz, M.H., Stokes, B.J., Eaton, L.M. (leads), *2016 Billion-Ton Report: Advancing Domestic Resources for a Thriving Bioeconomy, Vol. 1: Economic Availability of Feedstocks*, ORNL/TM-2016/160, Oak Ridge National Laboratory, USDOE, 2016.

45. International Energy Agency, *Energy Technology Perspectives 2017*, IEA, Paris, 2017.

Contacts

Eric Larson, elarson@princeton.edu
Clarence Lehman, lehman@umn.edu
David Tilman, tilman@umn.edu
Robert Williams, rwilliam@princeton.edu